ChemPubSoc Europe

DOI: 10.1002/ejoc.201501339

EurJOC European Journal of Organic Chemistry

Full Paper

Free-Radical Nitration

Nitropyrene Photoprobes: Making Them, and What Are They Good for?

Eli M. Espinoza,[a] Bing Xia,[b] Narek Darabedian,[c] Jillian M. Larsen,[d] Vicente Nuñez,[d][‡] Duoduo Bao,[d] Jenny T. Mac,[e] Fabian Botero,[e] Michelle Wurch,[d] Feimeng Zhou,[c] and Valentine I. Vullev*[a,d,e,f]

Abstract: Pyrene derivatives are among the most widely used organic fluorescent photoprobes. Many of them are photosensitizers for hole injection. Pyrenes, however, are mostly UV absorbers, limiting their utility for photonic applications. Nitration of pyrene shifts its absorption to the visible region. Conversely, nitration of pyrene that is already derivatized for covalent labeling, produces mixtures of isomers that are challenging to separate. We present a robust procedure for attaining isomerically pure nitropyrenes. NMR analysis provides unequivocal assignments of the regioisomers and of the structures of the disubstituted nitropyrenes. The added substituents negligibly affect the electronic properties of the nitropyrenes. Photoexcited nitropyrenes undergo efficient triplet formation, making them an attractive choice for triplet sensitizers and photooxidants. Hence, facile and reliable preparation of disubstituted nitropyrenes provides venues for exploring their electronic and photonic utility.

Introduction

This publication describes a robust procedure for preparation of nitropyrene-carboxyl derivatives that can be functionalized as aliphatic amines or carboxylates (Figure 1, Scheme 1). The principal challenge that we address is reproducible isolation of regioisomers of disubstituted nitropyrenes. Electrochemical and photophysical studies reveal that such functionalization causes minimal perturbation of the electronic properties of 1-nitropyrene (NPy).

Pyrene is one of the most broadly used and best-studied lipophilic photoprobes.[1] Referred to as nanographene,[2] pyrene is a polyaromatic hydrocarbon (PAH), comprising almost equal number of quaternary and tertiary carbons, i.e., about 40 % of its carbons are quaternary. At the edges, the tertiary carbons provide the chemical reactivity of this PAH. The π-conjugation, distributed over all carbons, governs its electronic and optical properties.

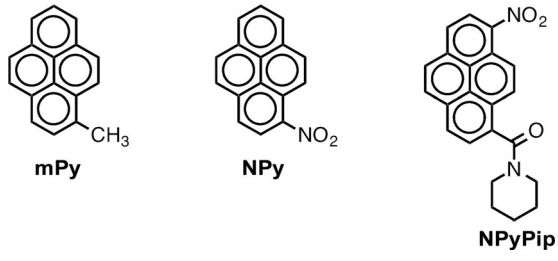

Figure 1. Structures of 1-methylpyrene (mPy), 1-nitropyrene (NPy) and (8-nitropyren-1-yl)(piperidin-1-yl)methanone (NPyPip).

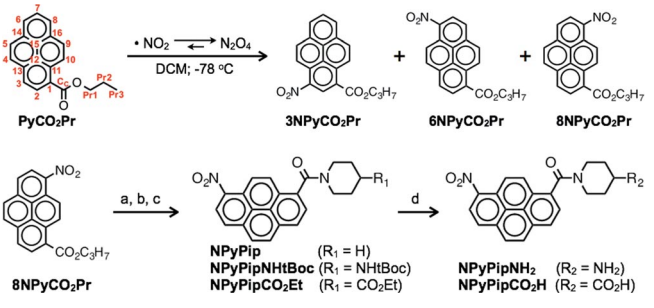

Scheme 1. Synthesis of disubstituted nitropyrenes. (a) KOH/C_2H_5OH, 60 °C; (b) $SOCl_2$, 80 °C; (c) $HN(CH_2CH_2)_2CH\text{-}R^1$; (d) F_3CCO_2H, room temp., if R^1 = NH*t*Boc; or KOH/C_2H_5OH, 60 °C, if $R^1 = CO_2Et$.

Similar to graphene sheets that form graphite, driven by π–π interactions, pyrenes self-assemble into supramolecular and nanometer-size structures with emerging photonic and elec-

[a] *Department of Chemistry, University of California, Riverside, CA 29521, USA*
E-mail: vullev@ucr.edu
http://www.vullevgroup.ucr.edu/
[b] *GlaxoSmithKline, MDR-Boston, Waltham, MA 02451, USA*
[c] *Department of Chemistry & Biochemistry, California State University, Los Angeles, CA 90032, USA*
[d] *Department of Bioengineering, University of California, Riverside, CA 29521, USA*
[e] *Department of Biochemistry, University of California, Riverside, CA 29521, USA*
[f] *Materials Science and Engineering Program, University of California, Riverside, CA 92521, USA*
[‡] Current address: Department of Neurobiology, Harvard Medical School, Boston, MA 02115, USA

Supporting information for this article is available on the WWW under http://dx.doi.org/10.1002/ejoc.201501339.

tronic properties.[3] This propensity for aggregation proves beneficial for forming quaternary structures of synthetic biomolecules.[4] Along with manifesting large fluorescence quantum yields and unusually long singlet-excited state lifetimes, the aggregation propensity of alkylpyrenes makes them unique photoprobes for monitoring interactions in lipophilic environment.[5] Changes in the color of the fluorescence of pyrene-labeled macromolecule from blue to green are an easily detectable indication for aggregation.[6]

Pyrene, however, absorbs in the near UV spectral region (300–350 nm), limiting its utility as a photoprobe to cases where selective UV photoexcitation is possible.[4a,7] Functionalizing pyrene with electron-donating and -withdrawing groups shifts its absorption toward the visible spectral region.[8] For example, electron-withdrawing (EW) groups, such as ketones or aldehydes, bring the pyrene absorption close to the edge between the UV and visible spectral regions.[7a,9] Nitropyrenes, containing an especially strong EW substituent, are yellow compounds with absorption that extends in the visible region of the spectrum, i.e., to wavelengths longer than 410 nm.[10] The mutagenicity and carcinogenicity of nitropyrenes have made them objects for biomedical and environmental research.[11]

Upon photoexcitation, nitropyrenes undergo efficient intersystem crossing (ISC) making these PAH derivatives excellent triplet photosensitizers.[10b] In parallel, the strong EW capabilities of the nitro group make nitropyrenes good electron acceptors.[10d] Alkyl substituents have negligible effect on the reduction potential of pyrene.[7a,7c] Replacing alkyl with alkanoyl substituents causes a 0.6-V positive shift in the reduction potential.[7a,9b] Conversely, replacing an alkyl substituent with a nitro group causes a positive shift exceeding 1 V.[11f,12]

These electronic characteristics make nitropyrenes unique photosensitizers. To utilize nitropyrenes as photoprobes and as building blocks for polymers and electronic materials, it is vital to provide a means for covalent conjugation without perturbing the effect of the EW nitro group. Substituted nitropyrenes present the simplest scenario for pursuing such venues of exploration, i.e., the nitro group governs the electronic properties of the PAH and the other functional group offers a means for covalent linking. Although it is the "simplest scenario," access to disubstituted nitropyrenes with sufficient regioisomeric purity is still limited.

Reduction to 4,5,9,10-tetrahydropyrene allows for adding functional groups at positions 2 and 7 with pronounced regioselectivity, which followed by re-oxidation, yields 2,7-disubstituted pyrenes.[13] The preparation of sufficiently pure 4,5,9,10-tetrahydropyrene, however, is challenging.[13a,14] Also, substituents at positions 2 and 7 do not have a strong electronic coupling with the pyrene π-conjugation[15] due to the nodal plane in the frontier orbitals.[16]

Pyrene has four sites for preferential aromatic substitution: positions 1, 3, 6, and 8 of this PAH (see $PyCO_2Pr$ on Scheme 1).[1a] Although this regioselectivity considerably simplifies the synthetic goals, nitration of 1-substituted pyrenes still yields mixtures of mainly three isomers (Scheme 1) that have relatively close chromatographic retention times. While nitration is well understood, doubly nitrated products or substitutions at positions 4, 5, 9, and 10, even under mild conditions, present further complications in the isolation of the targeted compounds.

Herein we present a facile procedure for preparing amino and carboxyl derivatives of nitropyrene with pronounced isomeric purity (Scheme 1). While normal-phase HPLC allows for efficient isolation of the various regioisomers, we employ solely "regular" column flash chromatography in the steps leading to the targeted compounds. Optimizing the procedures based on readily available techniques and establishing their reproducibility are important characteristics for the utility of the developed synthetic routes. We demonstrate unequivocal assignment of the exact positions of the nitro groups in the isolated isomers using a range of two-dimensional NMR techniques. Steady-state and time-resolved spectroscopy show that the carboxylamide linker does not significantly change the photophysical properties of the nitropyrene. Cyclic voltammetry reveal that the additional carboxylamide causes only a small positive shift (ca. 30-mV) in the reduction potential of nitropyrene.

Results and Discussion

Synthetic Routes

Carboxylates present a good choice for conjugating the targeted pyrene derivatives to macromolecules and other structures. While, 1-pyrenecarboxylic acid ($PyCO_2H$) is commercially available, it can also be readily prepared from pyrene via Friedel–Crafts acylation, followed by a haloform reaction.[17] Furthermore, the EW carbonyl of $PyCO_2H$ decreases the susceptibility of the pyrene ring to oxidation during the nitration step, resulting in a relatively clean mixture of products. $PyCO_2H$, however, has limited solubility in most organic solvents. Therefore, we protect the carboxyl as an ester, $PyCO_2R$, prior to nitration allowing it to proceed under relatively mild condition, e.g., –78 °C. In fact, limited solubility renders the utility of alternative routes, such as nitration of 1-acetylpyrene followed by haloform reaction, unfeasible.

Radical nitration of PAHs has received a great deal of attention because it allows for adopting mild reaction conditions and yields solely mononitrated products.[18] While cooling the reaction mixture decreases the solubility of pyrene conjugates, low temperature is favorable for these chemical transformations. The nitration mixture contains N_2O_4 and NO_2 that are in equilibrium. NO_2 is a reactive radical that can cause a range of undesired processes. Lowering the temperature shifts the equilibrium toward its dimer, N_2O_4 (Scheme 1), and allows for its "slow" release as it gets consumed by the desired nitration processes. Solutions of N_2O_4 in chlorinated media have blue color. An increase in the relative concentration of NO_2 (which is a brown gas) changes the color of such solutions to green. This feature is important for monitoring the reaction conditions. At room temperature the nitration mixture (NO_2 and N_2O_4 dissolved in dichloromethane) is green. It has to be cooled until it turns blue before adding it to the solution of the PAH starting material, which also should be maintained at the same low temperature. In addition to this thermodynamic effect, the low tem-

perature ensures the kinetic preference for the formation of mostly the isomers with a nitro group at position 3, 6 or 8.

Even when we implement low temperatures, the radical nitration of $PyCO_2R$ with N_2O_4/NO_2 proceeds to completion in relatively short times, resulting in quantitative yields of solely mononitrated isomers with the nitro group mainly at positions 3, 6, and 8 (Scheme 1, Figure 2, a, b). A detailed analysis, using Soxhlet-assisted extraction, reveals the formation of other mononitrated isomers (< 10 %) when the N_2O_4 solution is added fast, or the reaction mixture is not completely cooled down to the temperature of dry-ice/acetone bath (Figure 2, b).

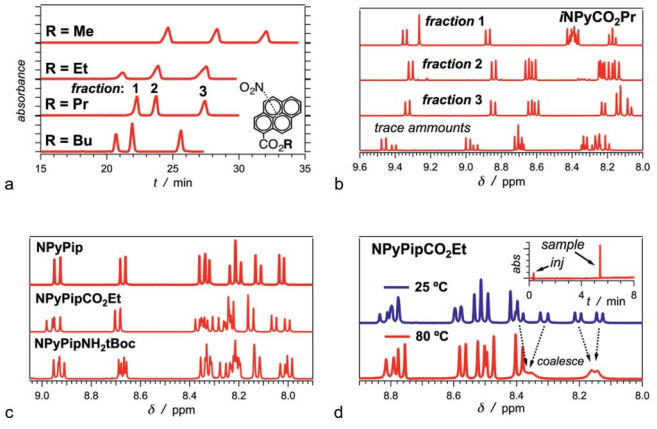

Figure 2. Analysis of the products at various stages of the preparation of the nitropyrene derivatives. (a) Chromatograms, monitored at 400 nm, from normal-phase HPLC tests of the nitration products of different esters of 1-pyrenecarboxylic acid, Me = methyl, Et = ethyl, Pr = *n*-propyl, and Bu = *n*-butyl (hexanes/ethyl acetate gradient, injection: 25 µL sample with 1 mg/mL concentration). (b) Aromatic region of ^{1}H-NMR spectra ($CDCl_3$) of the samples isolated from the three HPLC fractions of the nitrated propyl ester of 1-pyrenecarboxylic acid. The lowest spectrum is for the solid residue (< 5 %) remaining after extensive wash with hexanes (using Soxhlet apparatus) of $iNPyCO_2Pr$ mixture obtained from nitration when the N_2O_4 solution was not added slowly. (c) Aromatic region of ^{1}H-NMR spectra ($CDCl_3$) of NPyPip, and two derivatives, $NPyPipCO_2Et$ and $NPyPipNH_2tBoc$, that have a diasterogenic carbon. (d) Temperature dependence of ^{1}H-NMR spectra ($[D_6]$DMSO) of $NPyPipCO_2Et$, showing coalescence of some of the peaks. Inset: chromatogram, monitored at 400 nm, from LCMS analysis of $NPyPipCO_2Et$ showing, in addition to the injection (*inj*) signal, only a single sample peak (m/z = 431.1599, ascribed to $[M + H]^+$).

Facile isolation of a pure regioisomer is most important for the utility of this synthetic route. Therefore, the alkyl group, R, of the ester plays a crucial role in the design of the synthetic procedure. A short chain, e.g., R = CH_3 or C_2H_5, ensures that the exact position of the nitro group has a dominating effect on the chromatographic retention times of the isomers. The nitrated methyl and ethyl esters of the pyrenecarboxylic acid, however, have relatively low solubility in common organic solvents, leading to widened chromatographic peaks and bands (Figure 2, a), and limiting the amount of material that can be introduced in a column for separation. This limitation presents challenges to attempts for scaling up the preparation. Conversely, long flexible alkyl chains, R, immensely improve the solubility of the nitrated pyrene esters in organic solvents. This improved solubility and affinity for the eluent media, however, overwhelms the chromatographic discernibility between the regioisomers. That is, small ester substituents provide improved resolution but limit the amount of material that can be purified at each run. Large substituents allow for introducing large quantities of material in the chromatographic columns, at the cost of losing the resolution between some of the elution bands of the regioisomers.

Considering these opposing effects, we determined that substituents with intermediate size, such as *n*Pr and *n*Bu esters, provide an excellent compromise (Figure 2, a). Conversely, the aqueous wash after the alkaline hydrolysis of the purified isomers (Scheme 1) poses additional consideration for the procedure. The decrease in the molecular weight of aliphatic alcohols improves their water solubility, making the *n*-propyl ester, $PyCO_2Pr$ (Scheme 1), the preferred compromise for accommodating the opposing effects and requirements.

One of the three major regioisomers of the nitrated *n*-propyl ester (with the longest retention time) is well resolved chromatographically (Figure 2, a). In fact, using only flash chromatography allows for reproducible isolation of this well separated isomer in a single run. It is propyl 8-nitropyrene-1-carboxylate ($8NPyCO_2Pr$), as we assign using NMR analysis. Because of the relative ease of isolation of this particular disubstituted isomer, we base the rest of the procedures on it (Scheme 1). Hydrolysis of $8NPyCO_2Pr$ yields 8-nitropyrene-1-carboxylic acid, $NPyCO_2H$, which we conjugate with piperidine derivatives as potential linkers for photolabeling (Scheme 1). The piperidine derivative of the 8-nitropyrenecarboxyl, NPyPip, is a model for the chromophore in the prepared conjugates and we focus the electrochemical and photophysical studies on it.

Restricted bond rotation due to π-conjugation, results in diastereogenicity that causes splits in some of the chemical shifts. The pyperidinyl ^{1}H and ^{13}C NMR chemical shifts of NPyPip are consistent with "locked" conformers, i.e., NPyPip has five ^{13}C and six ^{1}H signals (with integration 1:1:2:2:2:2 protons) in the aliphatic NMR regions, instead of the expected three carbon and three proton signals (with integration 4:4:2 protons) for the symmetric pyperidine ring. This finding is not surprising for compounds containing amides or other bonds that are partially π-conjugated and the rotation around them is slower than the NMR spectroscopic data acquisition times. The observed number of NMR peaks, however, is smaller than what it would be expected for the two π-conjugated slow rotating bonds inducing this effect; i.e., (1) the bond between the pyrene C^1 carbon and the carbonyl carbon, C^C (Scheme 1); and (2) the amide bond. Indeed, extension of the π-conjugation along these two bonds stabilizes the planar structures. Rotation around the C^1–C^C bond leads to two planar (or close-to planar) conformers, i.e., *Z* and *E* (Scheme 2). The steric hindrance between the piperidinyl substituent with C^{10}–H^{10} of the pyrene rings makes the *E* conformer less favorable than the *Z* one (Scheme 2). While the *Z* conformer also has some overlap between the piperidinyl and the pyrene H^2 (Scheme 2), the steric hindrance is considerably more prohibitive for the *E* structure, suggesting that these conjugates exist predominantly in their *Z* configurations.

A functional group on the piperidinyl (Pip) ring, i.e., NPyPipR where R = NH_2, CO_2H, NHtBoc or CO_2Et (Scheme 1), causes additional splitting in the chemical shifts of the piperidine protons and carbons. Furthermore, in NPyPipR some of the pyrene

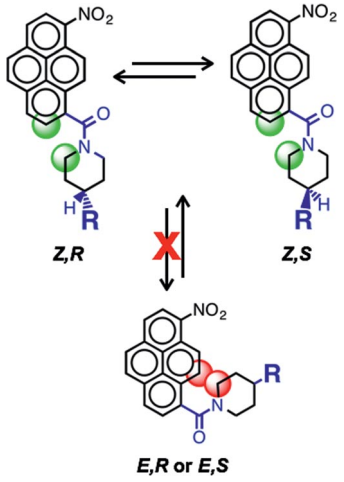

Scheme 2. Conformational transitions of NPyPipR. Green balls: overlaps between hydrogen atoms; red balls: overlaps between carbon–hydrogen bonds.

^{1}H and ^{13}C signals are split in comparison with those in NPyPip (Figure 2, c). The ^{1}H NMR spectra of the NPyPipR conjugates show up to 20-Hz splits in the signals of some of the aromatic protons (Figure 2, c, d). Concurrently, signals in the ^{13}C NMR spectra of the same compounds, recorded under ^{1}H-^{13}C decoupling, appear as doublets with up to 10-Hz splits. Elevating the temperature leads to coalescence of these split NMR peaks (Figure 2, d), which is consistent with accelerating the rotational modes around the partially π-conjugated bonds responsible for the observed patterns of the NMR signals. Because of the relative complexity of the NMR spectra, we employ liquid chromatography-mass spectrometry (LCMS) to further confirm the purity and the identity of the NPyPipR conjugates (see Supporting Information). Because the conformational dynamics, involving the restricted modes of bond rotation, is faster than the chromatographic timescales, all conjugates elute as single peaks, showing the corresponding *m/z* ratios (Figure 2, d, inset).

Because of the symmetry of the piperidine ring, a substituent on the carbon at the 4th position should not generate an enantiomeric center. Considering the whole structure, however, reveals that substituents on the 4th piperidinyl carbon induce axial chirality (Scheme 2) if the rotation around the amide bond is slow enough for the different conformers to appear as distinct species in the NMR spectra. While NMR spectroscopy cannot discern enantiomers, twists in the molecular structures (which are close to planar but not planar) induce additional asymmetries that make the substituents on the 4th piperidinyl carbon diastereogenic, affecting not only the aliphatic but also the aromatic ^{1}H and ^{13}C NMR signals.

Assigning the Nitro-Group Positions in the Regioisomers

The chromatographic fractions of the mixture of the nitrated propyl esters correspond to different regioisomers. The protons of each regioisomer exhibit distinctly different chemical shifts, making NMR spectroscopy a preferred tool for assigning the position of the nitro group. Indeed, for the sake of utility of the synthetic route, we are mainly interested in the isomer with longest retention time that is chromatographically well resolved. For completeness, however, we employ HPLC to isolate the three abundant isomers of the mononitrated propyl ester, and assign the positions of their nitro groups.

The patterns of coupling between the pyrene protons provide basic information for identifying the isomers of the mononitrated $PyCO_2Pr$. If the nitration is at position 6 or 8, the pyrene protons appear as eight doublets in the aromatic region of the ^{1}H NMR spectra. For a 7-nitro isomer, the aromatic protons also form eight doublets. The weak *meta*-coupling between H^6 and H^8 (*J* about 1 to 2 Hz), however, may make these two doublets appear as singlets in a case of peak broadening. Mononitration at the other position (i.e., 2, 3, 4, 5, 9, and 10) results in patterns comprising six doublets, a triplet (H^7), and a singlet (the proton next to the nitro group).

The isomer with the shortest retention time, i.e., from fraction 1 (Figure 2, a), exhibits a singlet at δ = 9.26 ppm and a triplet at δ = 8.17 ppm (Figure 2, b). As HMBC reveal, the three-bond coupling, ^{3}J, between the 9.26-ppm ^{1}H singlet and the carbonyl carbon of the ester (C^C) suggests that this isomer is the 3-nitro derivative, $3NPyCO_2Pr$ (see Supporting Information). While H^7 corresponds to the 8.17-ppm triplet, the proton next to the nitro group exhibits a singlet. Furthermore, the only possible $^{2}J_{C,H}$ or $^{3}J_{C,H}$ coupling of C^C with a pyrene proton is with H^2 (Scheme 1), validating the assignment of this isomer to $3NPyCO_2Pr$.

The other two isomers exhibit patterns of eight doublets in their aromatic regions (Figure 2, b), indicating that they are the 6- and 8-nitro derivatives. To assign the exact position of the nitro groups in these two isomers, we resort to two-dimensional (2D) NMR studies.[19] Correlation spectroscopy (COSY) reveals which protons are attached to neighboring carbons. ^{13}C-^{1}H HSQC spectroscopy shows to which carbon each proton is bonded, i.e., revealing single-bond coupling, $^{1}J_{C,H}$, patterns. ^{13}C-^{1}H HMBC spectroscopy relates chemical shifts of protons and carbons that are two- and three-bonds apart, i.e., $^{2}J_{C,H}$ and $^{3}J_{C,H}$ coupling, respectively.[19] For the aliphatic region, $^{2}J_{C,H}$ and $^{3}J_{C,H}$ coupling produce strong HMBC signals. For the pyrene (aromatic) region, the strong signals are only from $^{3}J_{C,H}$, while $^{2}J_{C,H}$ coupling yields weak or undetectable HMBC signals.

From the three major isomers, the one with the longest retention time, i.e., from fraction 3 (Figure 2, a), shows seven doublets in the aromatic region, one of which (at ca. 8.15 ppm) integrates to two protons (Figure 2, b). HMBC analysis confirmed that the most deshielded carbon, δ ca. 167 ppm, is the carbonyl one, C^C, which can exhibit $^{3}J_{C,H}$ only with H^{Pr1} and H^2 and cannot have any $^{2}J_{C,H}$ correlations (Scheme 1, Figure 3, c, d). These structural features allow for assigning the doublet at 8.7 ppm to H^2. From the chemical shift of H^2, COSY and HSQC allow for straightforward assignments of H^3, C^2, and C^3 (Figure 3, a, b).

Based on the structure (Scheme 1), H^3 should exhibit $^{3}J_{C,H}$ correlation with C^1, C^4 and C^{12}, of which C^1 and C^{12} are quaternary, i.e., they do not show HSQC $^{1}J_{C,H}$ signals. Furthermore, C^4 should manifest three-bond heteronuclear coupling only with one proton, H^3. If detectable, additional two HMBC signals for H^3 can originate from two-bond coupling with C^2 and C^{13}. From

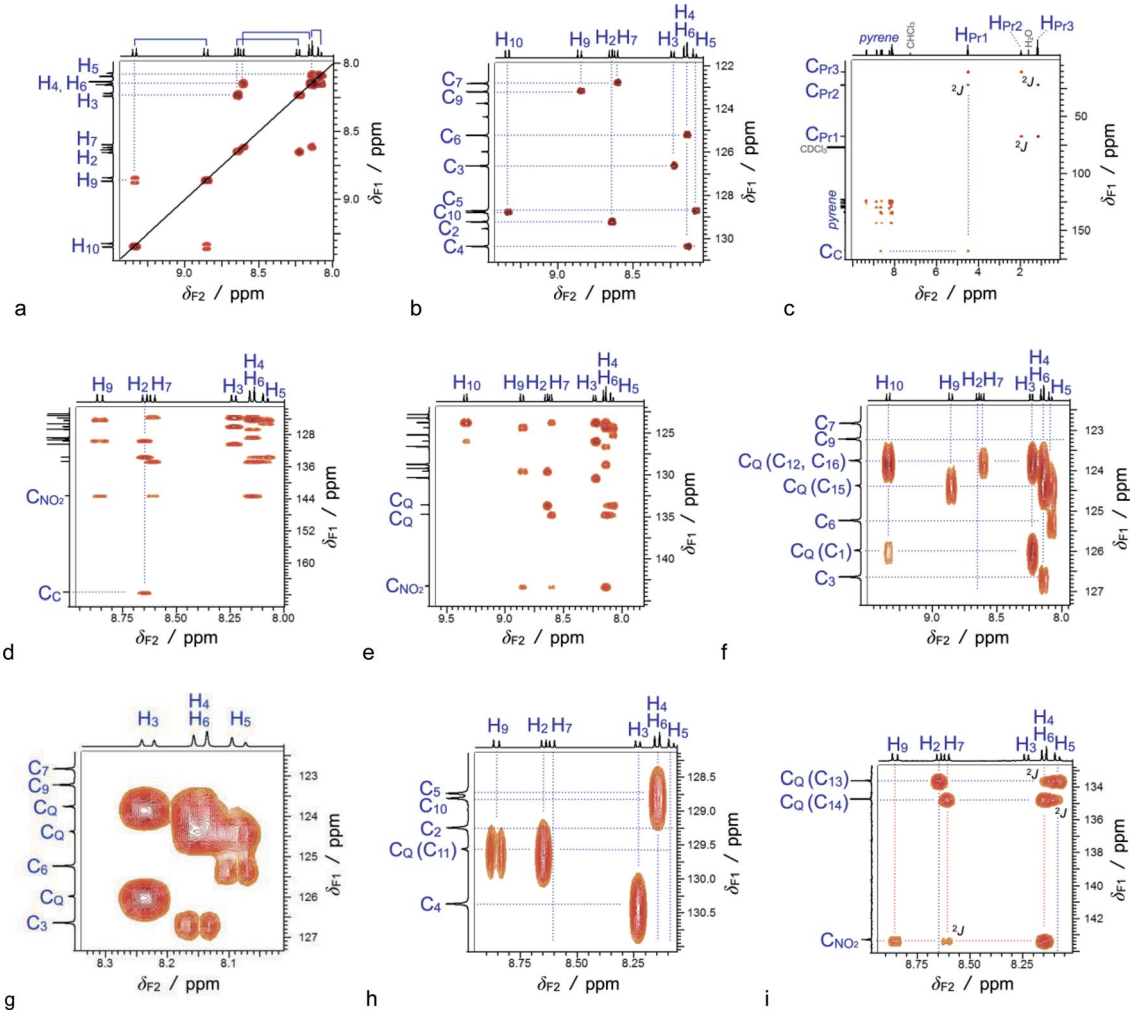

Figure 3. 2D NMR spectra of the third major chromatographic fraction (normal phase) of the nitrated propyl ester of the 1-pyrenecarboxylic acid. The spectra reveal that the nitro group is at the eighth position, allowing the assignment of this isomer as propyl 8-nitropyrene-1-carboxylate. Spectra of (a) COSY, showing $^{3}J_{H,H}$ coupling correlations, and (b) HSQC, showing $^{1}J_{C,H}$ coupling correlations, zoomed in the aromatic region with the assignments of the pyrene protons and tertiary carbons (Scheme 1). (c) HMBC spectrum showing the $^{3}J_{C,H}$ correlation between the propyl proton, H^{Pr1}, and carbonyl carbon, C^{C}. The four two-bond carbon-proton correlations in the aliphatic region (C^{Pr2}-H^{Pr1}, C^{Pr3}-H^{Pr2}, C^{Pr1}-H^{Pr2}, and C^{Pr2}-H^{Pr3}) are indicated with ^{2}J. (d–i) HMBC spectra zoomed in various aromatic regions, showing mostly $^{3}J_{C,H}$ correlations between the pyrene protons and: (1) the eight tertiary carbons, C^{2}–C^{7}, C^{9}, and C^{10}, (2) the seven quaternary carbons, C^{Q}: C^{1}, and C^{11}–C^{16}, (3) the carbonyl carbon, C^{C}, and (4) the carbon to which the nitrogroup is attached, C_{NO2}. (i) The relatively weak two-bond correlation observed for C^{13}, C^{14} and C_{NO2} are indicated with ^{2}J.

all five carbons that can exhibit $^{2}J_{C,H}$ or $^{3}J_{C,H}$ coupling with H^{3}, only C^{2} and C^{4} have protons directly attached to them, i.e., only C^{2} and C^{4} can show HSQC $^{1}J_{C,H}$ signals. HMBC experiments reveal that H^{3} has strong correlation signals with three carbons (Figure 3, d–h). Of these three, only the carbon with δ ca. 130.5 ppm shows $^{1}J_{C,H}$ HSQC signal, and it is not the already assigned C^{2} (Figure 3, b). Therefore, C^{4} is the only possibility for the carbon with δ ca. 130.5 ppm and, as HSQC signals show, one of the protons with the overlapping doublets at ca. 8.15 ppm is H^{4} (Figure 3, b). The remaining two H^{3}-correlated carbons (with δ ca. 124 and 126 ppm) can be assigned to C^{1} and C^{12}. Indeed, C^{13} can show a weak $^{2}J_{C,H}$ correlation with H^{3}, but it also has to have a strong $^{3}J_{C,H}$ HMBC signals with H^{2}. Neither the 124-ppm, nor the 126-ppm carbon shows HMBC correlation with H^{2}. Hence, neither of them is C^{13}. Both, C^{1} and C^{12}, are three bonds away from H^{10} (Scheme 1). In addition to H^{3}, only the most deshielded proton shows HMBC correlation with both, the 124-ppm and 126-ppm carbons (Figure 3, e, f), allowing for assigning H^{10}, H^{9}, C^{9}, and C^{10} (Figure 3, a, b).

The only possibility for $^{3}J_{C,H}$ coupling of C^{9} is with H^{8} (Scheme 1). C^{9}, however, does not exhibit any detectable HMBC signals (Figure 3, f), suggesting that H^{8} does not exist in this isomer, i.e., the nitro group is connected to C^{8}. Indeed, HMBC experiments did not show the two-bond coupling between C^{9} and H^{10} (Figure 3, f), which we attribute to the weak or undetectable nature of $^{2}J_{C,H}$ signals for the pyrene region in these HMBC experiments. Conversely, heteronuclear two-bond correlation (H2BC) spectroscopy,[20] which is optimized for $^{2}J_{C,H}$ coupling, shows strong correlation signals between C^{9} and H^{10}, confirming the assignments (see Supporting Information). Thus, the lack of correlation between C^{9} and H^{8} is not a result of a weak or undetectable signal; instead, it suggests that no proton is attached to C^{8}. Furthermore, H^{9} is three-bonds away from three carbons, C^{8}, C^{11} and C^{15}, of which only C^{11} and C^{15} are

quaternary (Scheme 1). None of the three carbons, with which H^9 shows HMBC signals (Figure 3, e, f, h, i), however, show $^1J_{C,H}$ coupling in HSQC (Figure 3, b), confirming that there is no proton attached directly to C^8, and the only possibility for the nitro group is to be at the eighth position, i.e., $C^8 = C_{NO2}$.

Following this train of thought, we assign all ^{13}C and ^1H chemical shifts (Figure 3). To test the robustness of this analysis, we examine alternative assignments where we assume that the nitro group is at the sixth position, i.e., $C^6 = C_{NO2}$. Such an assumption cannot account for a number of the correlations that are present in the NMR spectroscopic data. Concurrently, a similar NMR analysis allows for independent assignment of the isomer from fraction 2 to $6NPyCO_2Pr$ (see Supporting Information). Thus, the isomer from fraction 3, which we use for preparing the NPyPipR conjugates, is the 8-nitro derivative, $8NPyCO_2Pr$ (Scheme 1).

Because we use normal phase chromatography, it is reasonable to assume that this isomer, $8NPyCO_2Pr$, is more polar than $3NPyCO_2Pr$ and $6NPyCO_2Pr$. The nodal plane in the frontier orbitals is along the major H^3–C^3–C^{15}–C^{16}–C^7–H^7 axis,[16a,16b] splitting the pyrene π-conjugated system in two, where C^1 and C^8 are on one side and C^3 and C^6 – on the other. In $8NPyCO_2Pr$ both electron-withdrawing groups are on the same side, i.e., at positions one and eight, polarizing the pyrene rings and making this isomer the most polar of the three.

Electrochemical Reduction of Nitropyrenes

The reduction potentials of the nitropyrenes, as determined using cyclic voltammetery (CV), provide a means for evaluating their capability of these conjugates to act as electron acceptors. We focus on the CV behaviour of NPy and NPyPip (Figure 1), which allows for estimating the effect of the secondary amide on the reduction potential of this nitrated PAH.

For both nitropyrenes the cyclic voltammograms show cathodic waves at about –1 V vs. saturated calomel electrode (SCE) and second waves, twice larger than the first ones, at about –1.5 V vs. SCE (Figure 4, a, b). Reversing the sweeps right after the first cathodic waves yields anodic waves with comparable magnitude, which is indicative of reversible electrochemical reduction of the nitropyrenes (for aprotic media) if they are not over-reduced, e.g., if only a single electron is added to the LUMOs of these PAH conjugates.

The reversible waves, at about –1 V, show dependence on the concentration of the supporting electrolyte, C_{el}. An increase in C_{el} causes positive shifts in the potentials of the cathodic peaks (Figure 4, b), which is consistent with stabilization of the formed charged species, i.e., the nitropyrene radical anions, in media with an increased ionic strength.

Extrapolation to zero electrolyte concentration from the dependence of the half-wave potentials, $E^{(1/2)}$, on C_{el} provides estimates of the reduction potentials of the nitropyrenes for neat solvent, MeCN (Figure 4, c). The reduction potential of NPyPip is about 30 mV more positive than that of NPy. Hence, conjugating the nitrated pyrene with a carboxamide only slightly affects its electron-accepting properties.

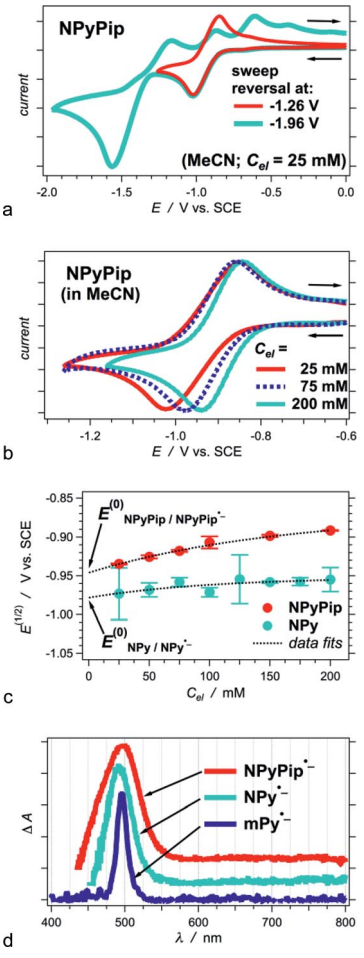

Figure 4. Electrochemical reduction of nitropyrenes in acetonitrile (MeCN) containing different amounts of supporting electrolyte, tetrabutylammonium hexafluorophosphate. (a) Cyclic voltammograms of NPyPip where the sweeps are reversed after the first cathodic wave (at about –1.2 V vs. SCE) and after the second wave (at about –2.0 V vs. SCE). (b) Cyclic voltammograms of NPyPip, reversed after the first cathodic waves, and recorded at different electrolyte concentrations, C_{el}. (a,b) for NPy see Supporting Information. (c) Dependence of the half-wave potentials, $E^{(1/2)}$, obtained from the first reduction waves of NPy and NPyPip, on the electrolyte concentration. Extrapolation to zero electrolyte concentration, C_{el} = 0, allows for estimating the reduction potentials, $E^{(0)}$, for neat solvent, MeCN.[21] (d) Differential absorption spectra recorded at the first cathodic waves of NPy, NPyPip and 1-methylpyrene (mPy, Figure 1) for MeCN, C_{el} = 100 mM.

Spectroelectrochemistry shows that the first reduction step of NPyPip and NPy leads to transients with similar absorption bands at about 500 nm (Figure 4, d). Coincidentally, the radical anion of alkylpyrenes, such as 1-methylpyrene (mPy), shows sharp absorption at about 500 nm.[7c] Furthermore, the radical anion of alkenoylpyrenes absorbs in the same region, showing a broad Δ*A* band at about 480 nm.[9b] This finding indicates that while π-conjugating substituents broaden the Δ*A* bands of pyrene radical anions, they do not alter the energy difference between the doublet states involved in the $D_1 \rightarrow D_{1+n}$ transition responsible for the observed transient absorption. These trends also suggest that the radical anion (spin density) of NPyPip is mainly localized on the pyrene polyaromatic ring system.

Photophysics of Nitropyrenes

The nitropyrenes, i.e., NPy and NPyPip, manifest absorption at the blue edge of the visible spectrum that extends to about 450 nm (Figure 5). A few recent reports demonstrate that NPy exhibits weak fluorescence with emission quantum yields in the order of 10^{-4}, and picosecond lifetimes.[10b,22] We examine this lead, and as attractive as the idea for fluorescent pyrene photoprobes susceptible to excitation with visible light is, our findings suggest that the observed emission does not originate from the nitropyrenes.

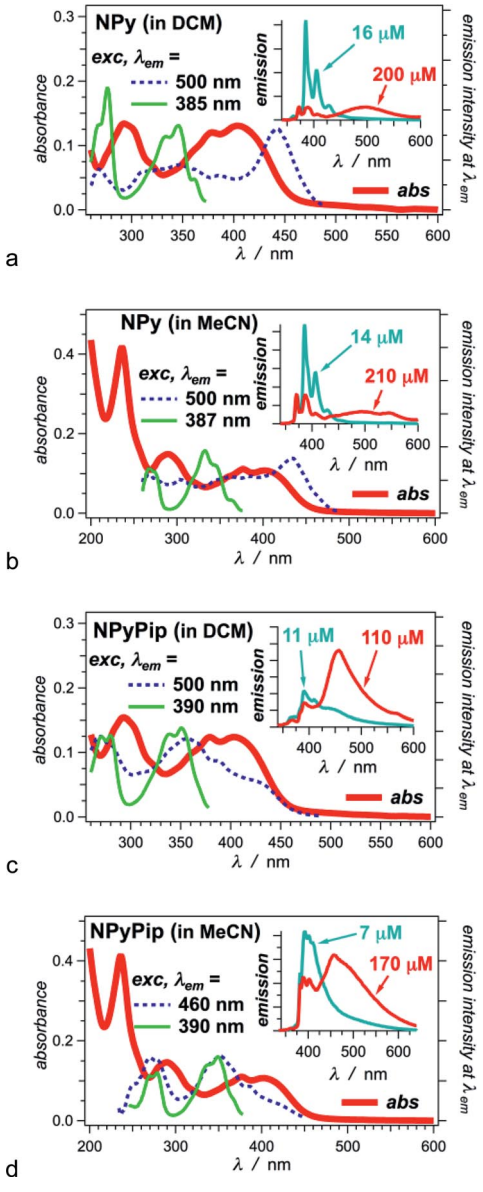

Figure 5. Absorption (*abs*), emission, and excitation (*exc*) spectra of NPy and NPyPip recorded for dichloromethane (DCM) and acetonitrile (MeCN) media. For the absorption spectra, the sample concentration is 10 μM. For the emission spectra (displayed in the insets, λ_{ex} = 325 nm) the sample concentration is designated. Excitation spectra are recorded while the emission intensity is monitored at different wavelengths, λ_{em}.

Indeed, when excited at about 400 nm, NPy and NPyPip manifest broad emission bands centered around 500 nm. The emission quantum yields (in the order of 10^{-4} and 10^{-3}), however, show dependence on sample concentration and on excitation wavelength, λ_{ex}. Moving λ_{ex} to the mid UV region, e.g., λ_{ex} = 325 nm, results in emission from the nitropyrene samples that has the spectral features of pyrene undergoing ground- or excited-state aggregation: i.e., sharp fluorescence with distinct vibronic features at about 400 nm, and a broad featureless band at about 500 nm (insets on Figure 5). For each sample, the ratio between the intensities of these 400-nm and 500-nm fluorescence bands is concentration dependent, which is evidence that the broad red-shifted emission is due to aggregation.[1b,4,23] The polarity dependence of the broad aggregate emission band is consistent with the formation of exciplexes or ground-state charge-transfer aggregates.[24]

The 400-nm fluorescence bands completely overlap with the absorption spectra of the samples. The emission at 400 nm, recorded for nitropyrenes, manifests biexponential decays with lifetimes of about 20 ns and 100 ns (see Supporting Information). Such singlet-excited-state lifetimes are typical for strongly fluorescent pyrene derivatives with quantum yields, φ_f, larger than about 0.1.[4c,9b,25] As evident from the transient absorption studies, presented below, NPy and NPyPip undergo efficient triplet formation in the picosecond time domain, with ISC rate constants that are orders of magnitude faster than the measured emission decay rates. Hence, unless emission originates from long-lived upper excited states that do not feed into the lowest signet excited state (which is absurdly unlikely), the observed 400-nm fluoresce cannot be from the nitropyrenes.

Excitation spectra further confirm this conclusion. Neither of them resembles the absorption of NPy or NPyPip regardless weather the emission, λ_{em}, is monitored at the red or the blue edges of the fluorescence spectra (Figure 5).

What is the origin of the observed fluorescence? Nitropyrenes are good electron acceptors that can undergo irreversible reduction (Figure 4, a). Hence, even the slightest reducing tendencies of the organic media that solubilizes the nitropyrenes may produce minute traces of fluorescent imputes. Strongly fluorescent impurities even at levels not exceeding 0.1 % can still account for φ_f in the order of 10^{-4} to 10^{-3}. All samples for these studies are, indeed, recrystallized and some are doubly recrystallized. The propensity of pyrene compounds for π–π stacking, however, may ensure that such impurities form ground-state charge-transfer aggregates with the abundant nitropyrenes in the samples, resulting in the red-shifted broad fluorescence bands that manifest solvatochromism.[26] The aggregation of the impurities would prevent their complete separation (using chromatography or recrystallization) from the principal nitropyrene components of the samples. At μM and nM sample concentrations, used for spectroscopic studies, the fluorescent trace compounds dissociated from the nitropyrenes exhibit the observed long-lived emission bands at 400 nm.

Upon photoexcitation, NPyPip and NPy form transients that have distinct overlapping absorption bands at about 440 and 500 nm (Figure 6, a, b). In addition, the NPyPip exhibits a weak broad band at about 600–700 nm, which is especially apparent for aprotic solvent media (Figure 6, a–c). Because this broad band at the red region of the spectrum is not detectable for

NPy, its appearance in this wavelength range is attributed to the amide of the NPyPip. Overall, the addition of the amide to the NPy causes slight red shifts in the transient absorption bands, consistent with extending the π-conjugation bringing closer the energy levels of the excited states responsible for the observed transitions (the spectra of NPy vs. NPyPip, Figure 6, c, d). These three transient-absorption bands (at about 440, 500 and 650 nm), ascribed to the singlet-excited state, form in the sub-picosecond time domain and have picosecond lifetimes.

For all samples, the 440-nm band is relatively narrow and its maximum remains stationary with time, suggesting that the energy gap between the states involved in the transition responsible for this absorption is conserved. Conversely, the band around 500 nm is relatively broad and manifests more than 20-nm blue shift as it grows and decays (Figure 6, a, b). Furthermore, the 500-nm band shows a strong dependence on the proticity, rather than on the polarity, of the media. For aprotic media, the band at about 500 nm dominates the transient spectra at the early femto- and picosecond time scales (Figure 6, a, c). The presence of protic solvents, however, weakens its relative intensity (Figure 6, b, c). A previous report ascribes the long-wavelength band (500 nm) to a conformer in which the nitro group is twisted and the short-wavelength band (440 nm) to a planar structure.[10c] The solvents we use, however, appears to prevent a clear a transition from the twisted to the planar excited-state conformer as it would have been expected for NPy.

The picosecond decay of the singlet-excited state transient absorption is concurrent with a growth of a broad feature with maxima at about 460, 530 and 570 nm (Figure 6, a, b). We ascribe this long-lived transient, with broad absorption bands, to the triplet state of the nitropyrenes (Figure 6, d).[10b,10c,22c]

For protic solvents, the decay rates of the S_1 440-nm band match the rise rates of the triplets (Figure 6, b, inset), hence, they are readily ascribed to the rates of intersystem crossing (ISC). For the aprotic solvents, however, where the 500-nm S_1 band is prevailing, the growth rates of the triplet transients do not appear to have an obvious match with the rates of the singlet decays (Figure 6, a, inset), therefore, we resort to multi-exponential global fits (see Supporting Information). For the aprotic solvents, the global fits allow for quantification of the ISC rates (Table 1). For the protic solvents, the rate constants of ISC are in agreement with the rates obtained from local fits, i.e., where each decay and rise curve are fitted individually (Table 1). For NPy, the global fits reveal some relatively slow rise components in the kinetics of triplet growth that do not necessarily match any of the decays of the 440-nm and 500-nm principal transient absorption bands of ^{1}NPy* (Table 1). These findings

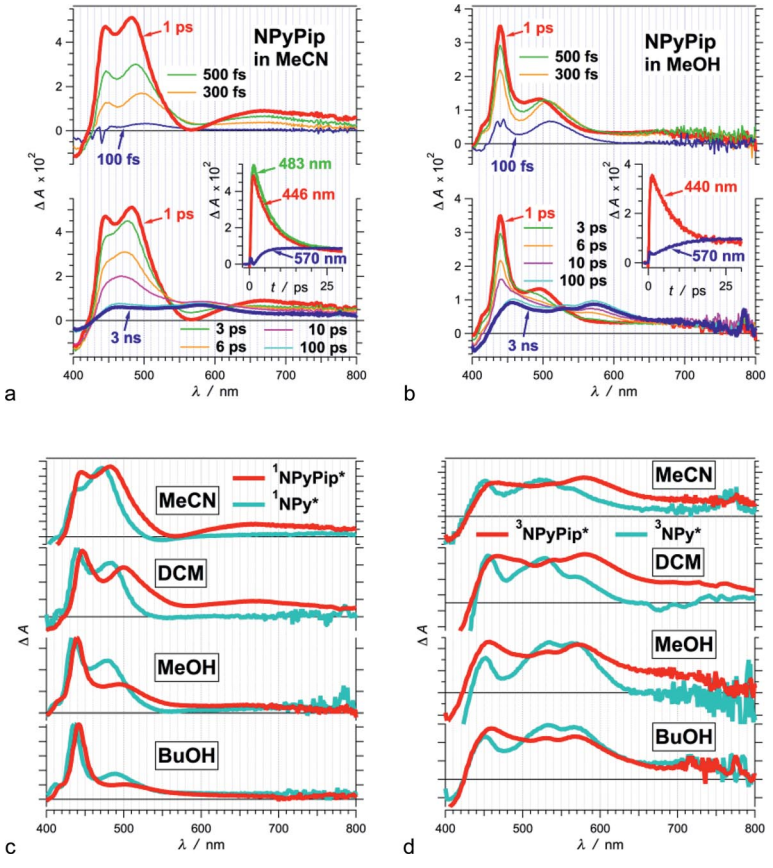

Figure 6. Transient absorption spectra of NPy and NPyPip for different solvents. (a,b) Spectra recorded at different times showing the growth and decay of the singlet-excited-state transient and the growth of the triplet transient of NPyPip for (a) acetonitrile (MeCN) and (b) methanol (MeOH). (c) Spectra of the singlet-excited-state transients of NPy and NPyPip, recorded 1 ps after the pump (excitation) pulse, for MeCN, dichloromethane (DCM), MeOH, and 1-butanol (BuOH).[27] (d) Spectra of the singlet-excited transients of NPy and NPyPip, recorded 0.1 to 3 ns after the pump pulse, for different solvents. (λ_{ex} = 390 nm; 50 fs pulse width at 800 nm, 4 μJ per pulse[27b,28]).

Table 1. Rates of decay of the singlet-excited states and of growth of the triplet states of NPy and NPyPip representing the kinetics of ISC.

	Solvent[a]	$^1k_d \times 10^{-10}$ / s^{-1} [b]	$^3k_r \times 10^{-10}$ / s^{-1} [c]	$^3k_r^{(GF)} \times 10^{-10}$ / s^{-1} [d]
NPy	MeCN	–	–	39.7 ± 1.3
	DCM	–	–	7.43 ± 5.4[e]
	MeOH	16.7 ± 0.4	16.2 ± 0.6	18.0 ± 0.3
				1.67 ± 0.13[e]
	BuOH	17.4 ± 1.9	18.6 ± 0.7	16.9 ± 0.2
				0.761 ± 0.086[e]
NPyPip	MeCN	–	–	28.5 ± 0.5
	DCM	–	–	19.6 ± 0.4
	MeOH	14.3 ± 0.1	13.8 ± 0.3	13.9 ± 0.1
	BuOH	12.4 ± 0.1	15.0 ± 0.4	13.0 ± 0.2

[a] Two aprotic solvents: acetonitrile (MeCN) and dichloromethane (DCM); and two protic solvents: methanol (MeOH) and 1-butanol (BuOH). MeCN and MeOH are relatively polar and with low viscosity, DCM and BuOH are relatively non-polar. BuOH has higher viscosity than the other three solvents. [b] Obtained from exponential fits of the Δ*A* decay of the peak situated between about 435 and 445 nm, ascribed to the singlet-excited state transient. [c] Obtained from exponential fits of the Δ*A* rise of the transient ascribed to the triplet excited state; recorded at 570 nm where the triplet absorption is significant and the singlet absorption is minimal. [d] Obtained from multiexponential global fits. The rate constants correspond to the rise components of the triplet transients, and they match principal decay compounds of the 440-nm transient-absorption bands. [e] For the protic solvents, 3NPy* shows also slow rise compounds that do not match any of decays the major 1NPy* bands between 430 and 550 nm; instead, the slow components match a decay at wavelength shorter than about 420 nm. Furthermore, the rate constant of the 3NPy* rise for DCM matches a decay component that is more prevalent in the 410-nm region than for the 440-nm and 500-nm bands (see Supporting Information).

suggest for multiple ISC pathways that seem to be eliminated by the amide substituent in NPyPip.

The nitropyrenes undergo efficient triplet formation with timeconstants ranging between about 3 and 10 ps. The solvent polarity does not have as apparent effect on the ISC kinetics as the proticity of the solvent media. Protic media appear to slow down the ISC. It is consistent with interfering with pathways involving states with n→π* character that become eliminated from the singlet-triplet transitions upon hydrogen bonding with the alcohols. This phenomenon is characteristic for certain carbonyl derivatives of pyrene, where hydrogen bonding shifts the energy of n→π* states suppressing triplet formation to allow fluorescence with adequate quantum yields.[9a] In the case of nitropyrenes, however, hydrogen bonding may impede, rather than eliminate, the ISC processes.

The spectral and electrochemical properties of nitropyrenes make them desirable photoprobes for triplet sensitization and for inducing a hole transfer by extracting an electron from neighboring electron donors. The latter feature is most likely the reason for the presence of traces of fluorescent impurities from the irreversible reduction of the nitropyrenes. Indeed, such minute amounts of fluorescent impurities appear to be inherent for any nitropyrene. Their presence, however, does not detectably affect the photodynamics of nitropyrenes as monitored with transient absorption spectroscopy (Figure 6), ensuring the utility of these nitrated PAHs as photonic agents for triplet formation and for initiation of charge transfer.

The excitation energy of nitropyrenes at the red edge of their absorption, corresponding to their "optical" HOMO–LUMO gap, is about 2.8 eV. The lowest triplet state, T_1, of NPy is about 1.6 eV above the ground state, S_0. While these energetics are about 200-meV shy from meeting a principal requirement for singlet fission, i.e., $E(S_1) \geq 2\ E(T_1)$,[29] further substituent tuning that may lower the energy of T_1 more than that of S_1, will lead to promising exploration of this class of chromophores in the quest for overcoming the Shockley and Queisser limit. In terms of considerations for singlet fission, nitropyrenes readily form crystalline solids and their excited states have a strong charge-transfer character.

Conclusions

The most crucial step in the synthetic route is the separation of the three regioisomers produced from the nitration (Scheme 1). The presented strategies focus on the preparing nitropyrenes with an aliphatic carboxyl or amine groups because of the pronounced utility of these two functionalities.[4a,7c,9b,30] We intentionally anchor the amine and carboxyl via a saturated linker to prevent their interference with the electronic properties of the nitropyrene chromophore. Indeed, carboxyls and amines are some of the most widely used groups for covalent photolabeling of biomolecules and polymers. Amine and carboxyl groups also provide a means for anchoring to inorganic chalcogenide and oxide surfaces, important for photonic and electronic hybrid materials.[28a,31] The electronic properties of nitropyrens make them attractive candidates for photonic application where photo-oxidation or transitions between singlet and triplet manifolds is important.

Experimental Section

Materials: 1-Pyrenecarboxylic acid, pyridine, ethyl 4-piperidinecarboxylate and 4-(*tert*-butoxycarbonylamino)piperidine were purchased from TCI America. 1-nitropyrene was purchased from Matrix Scientific. 4-(Dimethylamino)pyridine (DMAP) was purchased from Alfa–Aesar and thionyl chloride ($SOCl_2$) was purchased from Sigma–Aldrich. All other reagents (including HPLC grade, spectroscopic grade and anhydrous solvents) were purchased from Fisher Scientific.

General Synthesis Information: The NMR spectra were recorded at 400 MHz at ambient temperature (unless otherwise stated) using deuterated solvents, $CDCl_3$, [D_6]DMSO, [D_7]DMF, and CD_3OD. Chemical shifts are reported in parts per million relative to: $CDCl_3$ (^{1}H, δ = 7.241 ppm; ^{13}C, δ = 77.233 ppm), [D_6]DMSO (^{1}H, δ = 2.505 ppm; ^{13}C, δ = 39.517 ppm), [D_7]DMF (^{1}H, δ = 8.031 ppm; ^{13}C, δ = 163.153 ppm), and CD_3OD (^{1}H, δ = 3.315 ppm; ^{13}C, δ = 49.157 ppm). Data for ^{1}H NMR are reported as follows: chemical shift, integration, multiplicity (s = singlet, d = doublet, t = triplet, q = quartet, p = pentet/quintet, h = hextet/sextet, m = multiplet), and coupling constants. All ^{13}C NMR spectra were recorded with complete proton decoupling. High-resolution mass spectra (HRMS) were obtained using an Agilent LCTOF (6200) mass spectrometer (Agilent Technologies, Santa Clara, CA) and Exactive™ mass spectrometer (Thermo Fisher Scientific, Inc., San Jose, CA). Analytical thin layer chromatography (TLC) was performed using 0.25 mm silica gel 60-F plates. Flash chromatography was performed using 60 Å, 32–63 μm silica gel, yields refer to chromatographically pure materials, unless otherwise stated.

1-Propyl Pyrene-1-carboxylate ($PyCO_2Pr$): 1-Pyrenecarboxylic acid (500 mg, 2.0 mmol) and $SOCl_2$ (5 mL, 69 mmol) were mixed in a 50 mL round-bottomed flask, equipped to a water-cooled condenser, and immersed in a temperature controlled oil bath. The mixture was refluxed at 110 °C for 1 h. After cooling to room temperature, the liquid was evaporated from the solution until dry. DMAP (273 mg, 2.2 mmol) in propanol (3 mL, 40 mmol) was added to the chlorinated product. The mixture was refluxed at 110 °C and the progress of the reaction was monitored with TLC. Usually after an hour, no starting material was detected and a single green-fluorescent spot represented the major TLC-detectable component of the mixture. After cooling to room temperature, the clear solution was added dropwise in 100 mL of 1 % hydrochloric acid. White precipitate formed immediately. The precipitate was allowed to settle overnight and collected via filtration to yield (574 mg, 1.9 mmol, 98 %) of propyl $PyCO_2Pr$: ^1H NMR (400 MHz, $CDCl_3$): δ = 9.25 (d, J = 9.5 Hz, 1 H), 8.62 (d, J = 8.1 Hz, 1 H), 8.24 (m, 3 H), 8.17 (m, 2 H), 8.06 (m, 2 H), 4.46 (t, J = 6.7 Hz, 2 H), 1.92 (h, J = 7.1 Hz, 2 H), 1.12 (t, J = 7.4 Hz, 3 H) ppm. ^{13}C NMR ($CDCl_3$): δ = 168.31, 134.51, 134.48, 131.28, 130.84, 129.77, 129.59, 128.57, 127.41, 126.51, 126.48, 128.35, 125.16, 125.09, 124.47, 124.34, 61.44, 14.72 ppm. HRMS: m/z calculated $C_{20}H_{16}O_2$ M^+ 288.1138, found 289.1145 M^+.

Methyl Pyrene-1-carboxylate ($PyCO_2Me$): Following the procedure for $PyCO_2Pr$, while starting with 201 mg (0.82 mmol) 1-pyrenecarboxylic acid and treating the acyl chloride with methanol instead of propanol, produced 203 mg (0.78 mmol, 95 % yield) of $PyCO_2Me$: ^1H NMR (400 MHz, $CDCl_3$): δ = 9.24 (d, J = 9.4 Hz, 1 H), 8.61 (d, J = 8.2 Hz, 1 H), 8.22 (m, 3 H), 8.14 (d, J = 9.0 Hz, 1 H), 8.13 (d, J = 8.0 Hz, 1 H), 8.04 (m, 2 H), 4.09 (s, 3 H) ppm. ^{13}C NMR ($CDCl_3$): δ = 168.69, 134.53, 131.32, 131.20, 130.58, 129.81, 128.64, 128.61, 127.35, 126.49, 126.37, 126.10, 125.03, 124.39, 124.31, 123.67, 52.51 ppm. HRMS: m/z calculated $C_{18}H_{12}O_2$ $[M + H]^+$ 261.0912, found 261.091 $[M + H]^+$.

Ethyl Pyrene-1-carboxylate ($PyCO_2Et$): Following the procedure for $PyCO_2Pr$, while starting with 202 mg (0.82 mmol) 1-pyrenecarboxylic acid and treating the acyl chloride with ethanol instead of propanol, produced 203 mg (0.74 mmol, 90 % yield) of $PyCO_2Et$: ^1H NMR (400 MHz, $CDCl_3$): δ = 9.25 (d, J = 9.5 Hz, 1 H), 8.62 (d, J = 8.1 Hz, 1 H), 8.24 (m, 3 H), 8.17 (m, 2 H), 8.06 (m, 2 H), 4.56 (q, J = 7.1 Hz, 2 H), 1.52 (t, J = 7.1 Hz, 3 H) ppm. ^{13}C NMR ($CDCl_3$): δ = 168.31, 134.46, 131.26, 130.64, 129.77, 129.59, 128.57, 127.41, 126.51, 126.46, 126.35, 125.16, 125.09, 124.47, 124.34, 61.44, 14.72 ppm. HRMS: m/z calculated $C_{19}H_{14}O_2$ $[M + H]^+$ 275.1078, found 275.1067 $[M + H]^+$.

1-Butyl Pyrene-1-carboxylate ($PyCO_2Bu$): Following the procedure for $PyCO_2Pr$, while starting with 106 mg (0.43 mmol) 1-pyrenecarboxylic acid, produced 53 mg (0.17 mmol, 40 % yield) of $PyCO_2Bu$: ^1H NMR (400 MHz, $CDCl_3$): δ = 9.22 (d, J = 9.5 Hz, 1 H), 8.59 (d, J = 8.1 Hz, 1 H), 8.23 (m, 3 H), 8.14 (m, 2 H), 8.03 (m, 2 H), 4.48 (t, J = 6.6 Hz, 2 H), 1.85 (p, J = 7.4 Hz, 2 H), 1.56 (h, J = 7.6 Hz, 2 H), 1.01 (t, J = 7.4 Hz, 3 H) ppm. ^{13}C NMR ($CDCl_3$): δ = 168.42, 134.43, 131.23, 130.60, 129.72, 129.53, 128.51, 127.35, 126.47, 126.42, 126.30, 125.10, 125.05, 124.42, 124.29, 124.15, 65.35, 31.10, 19.63, 14.00 ppm. HRMS: m/z calculated $C_{21}H_{19}O_2$ $[M + H]^+$ 303.1380, found 303.1375 $[M + H]^+$.

Propyl Nitropyrene-1-carboxylates ($iNPyCO_2Pr$, i = 3, 6, 8): Dry dichloromethane (DCM) was chilled in a bath of dry ice and acetone. Nitrogen dioxide (NO_2) gas was produced from the oxidation of copper filings with concentrated nitric acid. To ensure that no traces of NO are present, the NO_2 stream was mixed with an excess of dry air and passed through the chilled DCM. The DCM solution turned blue due to the formation of N_2O_4. If the solution is warmed up, its color changes to green, due to the thermally induced shift in the equilibrium to NO_2 (i.e., to the decomposition N_2O_4). 12 mL of the cold N_2O_4 solution were added in small portions slowly, dropwise, to 10 mL of DCM solution containing $PyCO_2Pr$ (450 mg, 1.6 mmol), which was also pre-chilled in a bath of dry ice and acetone. The progress of the reaction was monitored with TLC, until the bright green fluorescent spot disappeared and two distinct yellow spots formed. (The yellow spots may or may not show very weak fluorescence.) The reaction mixture was added to a 100 mL of aqueous solution, saturated with $NaHCO_3$, and extracted with 50 mL of DCM. (***Caution:*** *Add the nitration reaction mixture slowly to the hydrogen carbonate solution, and carefully stir, to prevent splashing from violent formation of gaseous CO_2.*) The collected DCM solution was further washed with saturated solution of $NaHCO_3$ (2×50 mL), dried with anhydrous Na_2SO_4, and concentrated in vacuo to produce a yellow powder of a mixture of propyl nitropyrenecarboxyl isomers (423 mg, 1.3 mmol, 81 % crude yield). The mixture of the nitrited propyl pyrenecarboxylates (98 mg, 0.29 mmol) was purified using flash chromatography (stationary phase: silica gel; eluent gradient: from 100 % hexanes to 50 % ethyl acetate in hexanes) to afford 92 mg (93 % column yield) of bright yellow powder. NMR analysis showed that the yellow powder contained equal amounts $3NPyCO_2Pr$, $6NPyCO_2Pr$, and $8NPyCO_2Pr$, indicating that the nitration has equal selectivity for the positions 3, 6, and 8 of $PyCO_2Pr$: HRMS: m/z calculated $C_{20}H_{15}NO_4$ M^- 333.1001, found 333.0930 M^-.

1-Propyl 8-Nitropyrene-1-carboxylate ($8NPyCO_2Pr$): 102 mg of the crude nitration product, containing the iNPyCO$_2$Pr regioisomers, was subjected to flash chromatography (column, with 1″ internal diameter, was packed with silica gel in hexanes; 6″ to 8″ height of the packed stationary phase). Slow hexane/ethyl acetate gradient allowed separation of two principal yellow bands. The second eluted band was collected, tested with TLC to show a single yellow spot, and dried in vacuo to afford 21.5 mg (21 % column yield) of $8NPyCO_2Pr$: ^1H NMR (400 MHz, $CDCl_3$): δ = 9.33 (d, J = 10.0 Hz, 1 H), 8.85 (d, J = 10.0 Hz, 1 H), 8.64 (d, J = 8.1 Hz, 1 H), 8.60 (d, J = 8.4 Hz, 1 H), 8.22 (d, J = 8.1 Hz, 1 H), 8.14 (d, J = 8.7 Hz, 2 H), 8.08 (d, J = 8.9 Hz, 1 H), 4.48 (t, J = 6.7 Hz, 2 H), 1.94 (h, J = 7.1 Hz, 2 H), 1.14 (t, J = 7.4 Hz, 3 H) ppm. ^{13}C NMR ($CDCl_3$): δ = 167.63, 143.54, 134.95, 133.84, 130.59, 129.78, 129.47, 129.03, 128.96, 126.87, 126.20, 125.46, 124.60, 123.97, 123.43, 123.04, 67.51, 22.43, 10.97 ppm. HRMS: m/z calculated $C_{20}H_{15}NO_4$ $[M + H]^+$ 334.1074, found 334.1080 $[M + H]^+$.

Propyl 3-Nitropyrene-1-carboxylate ($3NPyCO_2Pr$): 40 mg of the nitration product, containing the iNPyCO$_2$Pr regioisomers, which was purified with flash chromatography, were dissolved in 1 mL of DCM, was loaded and injected (in several runs) in an HPLC equipped with a normal-phase semi-preperative column. Hexanes/ethyl acetate gradient (0.33 %/min, starting with 99.5 % hexanes, at flow rate of 10 mil/min) was applied. The first yellow fraction was collected and dried in vacuo to produce 12 mg (30 % HPLC column yield) of $3NPyCO_2Pr$: ^1H NMR (400 MHz, $CDCl_3$): δ = 9.35 (d, J = 9.4 Hz, 1 H), 9.26 (s, 1 H), 8.88 (d, J = 9.4 Hz, 1 H), 8.40 (m, 4 H), 8.17 (t, J = 7.6 Hz, 1 H), 4.49 (t, J = 6.7 Hz, 2 H), 1.94 (h, J = 7.2 Hz, 2 H), 1.12 (t, J = 7.4 Hz, 3 H) ppm. ^{13}C NMR ($CDCl_3$): δ = 166.53, 142.23, 1134.78, 133.63, 132.77, 130.44,130.27, 129.04, 128.69, 127.74, 127.32, 125.76, 125.34, 124.77, 123.60, 123.40, 121.61, 67.75, 22.39, 10.91 ppm.

1-Propyl 6-Nitropyrene-1-carboxylate ($6NPyCO_2Pr$): Following the procedure for $3NPyCO_2Pr$, and collecting the second HPLC yellow fraction, resulted in in 11 mg (28 % HPLC column yield) of $6NPyCO_2Pr$: ^1H NMR (400 MHz, $CDCl_3$): δ = 9.31 (d, J = 9.4 Hz, 1 H),

8.84 (d, *J* = 9.4 Hz, 1 H), 8.65 (d, *J* = 8.1 Hz, 1 H), 8.62 (d, *J* = 8.4 Hz, 1 H), 8.24 (d, *J* = 8.1 Hz, 1 H), 8.23 (d, *J* = 9.5 Hz, 1 H), 8.18 (d, *J* = 8.5 Hz, 1 H), 8.15 (d, *J* = 9.4 Hz, 1 H), 4.48 (t, *J* = 6.7 Hz, 2 H), 1.93 (h, *J* = 7.1 Hz, 2 H), 1.13 (t, *J* = 7.4 Hz, 3 H) ppm. ^{13}C NMR ($CDCl_3$): δ = 167.72, 143.84, 134.20, 132.97, 131.26, 130.80, 129.43, 128.78, 128.32, 126.72, 126.39, 125.45, 124.71, 124.54, 123.69, 123.05, 67.49, 22.42, 10.96 ppm.

Methyl Nitropyrene-1-carboxylate (iNPyCO$_2$Me, regio isomers): Following the procedure for *i*NPyCO$_2$Pr, while starting with 25.8 mg PyCO$_2$Me (0.094 mmol), after flash-chromatography column, resulted in 18 mg (0.059 mmol) of yellow powder (63 % yield) of a mixture of *i*NPyCO$_2$Me regioisomers: HRMS: *m/z* calculated $C_{18}H_{12}NO_4$ $[M + H]^+$ 306.0761, found 306.0700 $[M + H]^+$.

Ethyl Nitropyrene-1-carboxylate (iNPyCO$_2$Et, regio isomers): Following the procedure for *i*NPyCO$_2$Pr, while starting with 24.5 mg PyCO$_2$Et (0.089 mmol), after flash-chromatography column, resulted in 24 mg (0.075 mmol) of yellow powder (85 % yield) of a mixture of *i*NPyCO$_2$Et regioisomers: HRMS: *m/z* calculated $C_{19}H_{14}NO_4$ $[M + H]^+$ 320.0917, found 320.0900 $[M + H]^+$.

Butyl Nitropyrene-1-carboxylate (iNPyCO$_2$Bu, regio isomers): Following the procedure for *i*NPyCO$_2$Pr, while starting with 130 mg PyCO$_2$Bu (0.43 mmol), after flash-chromatography column, resulted in 142 mg (0.408 mmol) of yellow powder (95 % yield) of a mixture of *i*NPyCO$_2$Bu regioisomers: HRMS: *m/z* calculated $C_{21}H_{18}NO_4$ $[M + H]^+$ 348.1230, found 348.1200 $[M + H]^+$.

8-Nitropyrene-1-carboxylic Acid (NPyCO$_2$ H): Potassium hydroxide (400 mg) was dissolved in 3.6 mL of ethanol and added to a round-bottomed flask containing 8NPyCO$_2$Pr (300 mg, 0.90 mmol) already dissolved in 3.6 mL of ethanol. The solution was heated to 75 °C and the progress of the hydrolysis was monitored with TLC. After the reaction was completed (after about 30 min of heating) the ethanol was evaporated in vacuo. The remaining solid was suspended in small mount of ethanol and added drop wise to 100 mL of 5 % HCl. The formed yellow precipitate was allowed to settle overnight and collected via filtration to produce 250 mg orange solid (0.86 mmol, 95 % yield) of NPyCO$_2$H: ^{1}H NMR (400 MHz, [D$_6$]DMSO): δ = 9.40 (d, *J* = 9.1 Hz, 1 H), 8.77 (d, *J* = 9.9 Hz, 1 H), 8.76 (d, *J* = 8.4 Hz, 1 H), 8.69 (d, *J* = 8.0 Hz, 1 H), 8.54 (d, *J* = 8.6 Hz, 1 H), 8.52 (d, *J* = 8.6 Hz, 1 H), 8.47 (d, *J* = 8.9 Hz, 1 H), 8.42 (d, *J* = 8.9 Hz, 1 H) ppm. ^{13}C NMR ([D$_6$]DMSO): δ = 168.24, 143.12, 134.55, 133.23, 130.81, 129.37, 128.91, 128.68, 128.66, 127.34, 126.81, 128.11, 123.59, 123.07, 123.02, 122.75, 122.54 ppm. HRMS: *m/z* calculated $C_{17}H_9N_1O_4$ M^- 291.0549, found 291.0537 M^-.

(8-Nitropyren-1-yl)(piperidin-1-yl)methanone (NPyPip): NPyCO$_2$H (55 mg, 0.15 mmol) was dissolved in $SOCl_2$ (0.5 mL, 6.9 mmol) in a 50 mL round-bottomed flask equipped to a water-cooled condenser and immersed in a temperature controlled oil bath. The mixture was heated at 80 °C for 3 h. After cooling to room temperature, $SOCl_2$ was evaporated from the solution until dryness. The acyl halide was dissolved in dry DCM and chilled in a water ice bath. Piperdine (51 µL, 0.42 mmol) in dry DCM was added to the acyl halide solution and heated overnight at 45 °C under nitrogen gas. After acid wash, the organic phase was collected and the product was purified using flash chromatography (stationary phase: 90 % silica gel and 10 % potassium carbonate; eluent gradient: from 100 % DCM to 75 % methanol in DCM). The sample was then recrystallized twice from ethanol to afford 27 mg of yellow crystalline material (0.076 mmol, 49 % yield) of NPyPip: ^{1}H NMR (400 MHz, $CDCl_3$): δ = 8.94 (d, *J* = 9.7 Hz, 1 H), 8.67 (d, *J* = 8.5 Hz, 1 H), 8.33 (m, 2 H), 8.22 (m, 2 H), 8.12 (d, *J* = 8.9 Hz, 1 H), 8.02 (d, *J* = 7.8 Hz, 1 H), 4.02 (p, *J* = 6.0 Hz, 1 H), 3.92 (p, *J* = 6.1 Hz, 1 H), 3.12 (t, *J* = 5.6 Hz, 2 H), 1.81 (t, *J* = 5.5 Hz, 2 H), 1.70 (dq, *J* = 10.8, 5.3 Hz, 2 H), 1.41 (p, *J* = 5.7 Hz, 2 H) ppm. ^{13}C NMR ($CDCl_3$): δ = 168.89, 143.43, 135.40, 134.25, 131.43, 130.81, 128.47, 127.77, 127.70, 126.72, 125.13, 125.05, 124.79, 124.04, 123.25, 123.11, 48.74, 43.25, 26.91, 26.11, 24.74 ppm. HRMS: *m/z* calculated $C_{22}H_{18}N_2O_3$ $[M - H]^-$ 357.1248, found 357.1234 $[M - H]^-$.

***tert*-Butyl-[1-(8-nitropyrene-1-carbonyl)piperidin-4-yl] Carbamate (NPyPipNHtBoc):** Following the procedure for NPyPip, using 53.3 mg of NPyCO$_2$H (0.183 mmol), 4-(*tert*-butoxycarbonylamino)piperidin (0.3 mmol) and DMAP (45 mg, 0.369 mmol), instead of piperdine, afforded 66.2 mg (0.153 mmol, 83.6 % yield after recrystallization) of MPyPipNHtBoc (LCMS reveals a single chromatographic peak): ^{1}H NMR (400 MHz, $CDCl_3$): δ = 8.93 (dd, *J* = 9.6, 7.8 Hz, 1 H), 8.67 (dd, *J* = 8.5, 4.0 Hz, 1 H), 8.33 (m, 1.5 H), 8.27 (d, *J* = 9.7 Hz, 0.5 H), 8.22 (ddd, *J* = 8.4, 5.7, 2.4 Hz, 2 H), 8.13 (m, 1 H), 8.01 (m, 1 H), 4.91 (t, *J* = 15 Hz, 1 H), 4.53 (m, 1 H), 3.72 (s, 1 H), 3.31 (m, 1 H), 3.09 (m, 2 H), 2.18 (m, 1 H), 1.66 (m, 3 H), 1.41 (d, *J* = 4.7 Hz, 9 H) ppm. ^{13}C NMR ($CDCl_3$): δ = 168.99, 155.25, 155.22, 143.48, 143.42, 135.40, 135.36, 133.57, 133.47, 131.64, 131.56, 130.83, 130.74, 128.16, 128.11, 127.96, 127.93, 127.74, 127.67, 126.74, 126.69, 125.30, 125.06, 124.89, 124.70, 124.06, 123.99, 123.39, 123.34, 123.26, 48.08, 46.65, 46.38, 41.24, 41.13, 33.67, 32.78, 32.56, 28.58 ppm. HRMS: *m/z* calculated $C_{27}H_{27}N_3O_5$ $[M + H]^+$ 474.2024, found 474.2023 $[M + H]^+$.

(4-Aminopiperidin-1-yl)(8-nitropyren-1-yl)methanone (NPyPipNH$_2$): NPyPipNHtBoc (30 mg, 0.063 mmol) was dissolved in 1 mL of trifluoroaceticacid (TFA) and stirred for 1 h. TFA was evaporated to afford 22 mg (0.060 mmol, 94 % yield) of NPyPipNH$_2$ (LCMS reveals a single chromatographic peak): ^{1}H NMR (400 MHz, CD_3OD): δ = 8.86 (dd, *J* = 15, 9.6 Hz, 1 H), 8.68 (dd, *J* = 8.4, 6.0 Hz, 1 H), 8.50 (d, *J* = 7.8 Hz, 1 H), 8.37 (m, 2.5 H), 8.27 (m, 1.5 H), 8.12 (dd, *J* = 14, 7.8 Hz, 1 H), 5.05 (t, *J* = 11 Hz, 1 H), 3.45 (m, 2 H), 3.23 (m, 2 H), 2.28 (m, 1 H), 1.84 (m, 2 H), 1.54 (m, 1 H) ppm. ^{13}C NMR (CD_3OD): δ = 171.17, 145.02, 136.58, 133.75, 133.34, 131.82, 131.75, 129.34, 129.02, 128.97, 128.66, 127.86, 126.94, 126.90, 126.26, 126.10, 125.91, 125.24, 124.28, 124.18, 54.95, 47.07, 46.77, 41.49, 41.39, 31.97, 31.59, 31.21, 31.03 ppm. HRMS: *m/z* calculated $C_{22}H_{19}N_3O_3$ $[M + H]^+$ 374.1426, found 374.1435 $[M + H]^+$.

Ethyl 1-(8-Nitropyrene-1-carbonyl)piperidine-4-carboxylate (NPyPipCO$_2$Et): Applying the procedure for NPyPip, using 57 mg of NPyCO$_2$H (0.196 mmol) and ethyl 4-piperidinecarboxylate instead of piperdine afforded 66 mg (0.15 mmol, 78 % yield) of NPyPipCO$_2$Et (LCMS reveals a single chromatographic peak): ^{1}H NMR (400 MHz, $CDCl_3$): δ = 8.95 (dd, *J* = 13, 9.7 Hz, 1 H), 8.69 (d, *J* = 8.4 Hz, 1 H), 8.34 (m, 2 H), 8.24 (m, 2 H), 8.15 (d, *J* = 8.8 Hz, 1 H), 8.03 (dd, *J* = 22, 7.8 Hz, 1 H), 4.79 (m, 1 H), 4.15 (q, *J* = 7.1 Hz, 2 H), 3.36 (m, 1 H), 3.26 (m, 1 H), 3.04 (m, 1 H), 2.59 (m, 1 H), 2.17 (dt, *J* = 8.9, 4.5 Hz, 1 H), 1.94 (m, 1 H), 1.70 (m, 1 H), 1.61 (m, 1 H), 1.25 (td, *J* = 7.1, 2.7 Hz, 3 H) ppm. ^{13}C NMR (CD_3OD): δ = 174.25, 174.08, 169.04, 135.39, 133.61, 131.61, 131.57, 130.81, 130.76, 128.23, 128.19, 127.93, 127.76, 127.63, 126.81, 126.67, 125.26, 125.09, 125.02, 124.71, 124.06, 124.00, 123.37, 123.31, 61.00, 47.03, 46.81, 41.52, 41.14, 41.12, 29.06, 28.73, 28.33, 14.42 ppm. HRMS: *m/z* calculated $C_{25}H_{22}N_2O_5$ $[M + H]^+$ 431.1613, found 431.1601 $[M + H]^+$.

1-(8-Nitropyrene-1-carbonyl)piperidine-4-carboxylic Acid [5c, (NPyPipCO$_2$H)]: NPyPipCO$_2$Et (10.8 mg, 0.025 mmol) was dissolved in 4.5 mL of 1 M solution of KOH in ethanol in a round-bottomed flask equipped to a water-cooled condenser and immersed in a temperature controlled oil bath. The mixture was heated to 75 °C for one hour. The solution was added to 50 mL of 5 % hydrochloric acid and the formed precipitate was collected using filtration, to yield 7.7 mg (0.019 mmol, 76 % yield) of NPyPipCO$_2$H (LCMS reveals

a single chromatographic peak): ^{1}H NMR (400 MHz, [D$_7$]DMF): δ = 12.62 (br. s, 1 H), 8.95 (dd, J = 15, 9.6 Hz, 1 H), 8.84 (d, J = 8.6 Hz, 1 H), 8.65 (dd, J = 7.8, 3.1 Hz, 1 H), 8.58 (m, 2.5 H), 8.45 (m, 1.5 H), 8.25 (dd, J = 34.7, 7.8 Hz, 1 H), 4.75 (m, 1 H), 3.37 (m, 1.5 H), 3.21 (m, 1.5 H), 2.70 (m, 1 H), 2.17 (dd, J = 13.3, 2.7 Hz, 1 H), 1.95 (m, 0.5 H), 1.79 (m, 1.5 H), 1.65 (q, J = 9.4 Hz, 0.5 H), 1.53 (q, J = 9.4 Hz, 0.5 H) ppm. ^{13}C NMR ([D$_7$]DMF): δ = 176.67, 168.92, 144.37, 138.40, 135.64, 132.35, 131.97, 129.83, 129.55, 129.13, 129.04, 128.84, 127.47, 126.74, 126.44, 126.31, 125.54, 124.99, 124.52, 124.45, 124.23, 123.43, 105.66, 47.71, 47.45, 41.98, 41.84, 41.63, 29.77, 29.26, 29.21 ppm. HRMS: m/z calculated $C_{23}H_{18}N_2O_5$ [M + H]$^+$ 403.1216, found 403.1296 [M + H]$^+$.

High Performance Liquid Chromatography (HPLC): Normal-phase analysis was performed using HPLC System Gold from Beckman, equipped with analytical (4.6 mm × 250 mm) and semipreparative (11 mm × 250 mm) columns, packed with silica (5 μm). For the analytical settings (Figure 2, a), hexanes/ethyl acetate gradient (1 %/mL) was applied with flow rate of 1 mL/min. For the LCMS analysis (Figure 2, d, inset), reverse-phase HPLC was employed, using a Kinetex C18 column (1.7 μm, 2.0 mm × 50 mm, 100 Å) from Phenomenex (Torrance, CA) with a flow rate of 0.5 mL/min at 40 °C. The mobile phase contained water and acetonitrile with 0.1 % formic acid (V/V). The gradient was ramped from 5 % to 95 % acetonitrile over 7 min, returned from 95 % to 5 % over 0.5 min, and maintained at 5 % acetonitrile for 2.5 min prior to next injection.

Electrochemical Measurements: Cyclic voltammetry (CV) was conducted using Reference 600^{TM} Potentiostat/Galvanostat/ZRA (Gamry Instruments, PA, U.S.A.), equipped with a three-electrode cell. The half-wave reduction potentials, $E^{(1/2)}$, of the nitropyrenes were obtained from cyclic voltammograms recorded for samples of the analytes (1 to 5 mM) dissolved in dry acetonitrile containing different concentrations, C_{el}, of supporting electrolyte, tetrabutylammonium hexafluorophosphate. Prior each measurements, the surfaces of the glassy carbon working electrode was cleaned and dried, and the solution was purged with high-purity argon. During the measurements, the stream of argon was allowed to blanket the solutions without stirring them. From the dependence of $E^{(1/2)}$ on C_{el}, extrapolations to zero electrolyte concentration provided estimates of the reduction potentials, $E^{(0)}$, for acetonitrile (Figure 4, c). The SCE reference electrode was connected to the cell via salt bridges, and CV of ferrocene samples (before and after each series of measurements) provided a means for correcting for potential drifts (usually, less than 50 mV), due to diffusion of water miscible organic solvents into the reference electrode. The SCE electrode is stored in freshly prepared saturated KCl solution in MilliQ water.

For spectroelectrochemical measurements, a three-electrode cell was assembled in a 10-mm×10-mm quartz cuvette, the bottom 5 mm of which narrowed to 2-mm×10-mm. UV/Vis light source and a CCD spectrometer were connected with the cuvette holder via optical fibers. The working electrode, platinum mesh, was placed in the 2-mm×10-mm confined section at the bottom of the cuvette and the light beam was aligned to pass through the mesh. Platinum and silver wires were used for a counter and pseudoreference electrodes, respectively. The latter was calibrated with ferrocene samples. The intensities, $I(E)$, of the light passing through the sample and the working electrode were recorded at different potentials, E, while sweeping the voltage. The change in the absorbance, ΔA, for each potential, corresponding to the spectra of the electrochemically reduced species, i.e., radical anions of the nitropyrenes, was calculated in respect with the intensity at 0 V vs. the reference, $\Delta A(E) = \log [I(0)/I(E)]$.

UV/Vis absorption and Emission Spectroscopy: Steady-state absorption spectra were recorded in a transmission mode using a JASCO V-670 spectrophotometer (Tokyo, Japan); and steady-state emission and excitation spectra were measured, also in a transmission mode, with a FluoroLog-3 spectro-fluorometer (Horiba–Jobin–Yvon, Edison, NJ, USA).

Time correlated single photon counting (TCSPC) measurements were also carried out using the FluoroLog-3 instrument, which was equipped with a UV diode (278 nm) as a pulsed excitation source, run at 250 kHz frequency. Decays were recorded at different emission wavelengths, λ_{em}, corresponding to the monomer (λ_{em} ca. 400 nm) and aggregate (λ_{em} ca. 500 nm) fluorescence as revealed on the steady-state spectra. The emission lifetimes were obtained from biexponential data fits.

Transient Absorption Spectroscopy: The transient-absorption data (Figure 6) were recorded in transmission mode with 2-mm quartz cuvettes using a Helios pump-probe spectrometer (Ultrafast Systems, LLC, Florida, USA) equipped with a delay stage allowing maximum probe delays of 3.2 ns at 7 fs temporal step resolution. Immediately prior the measurements, all samples were purged with argon. The laser source for the Helios was a SpitFire Pro 35F regenerative amplifier (Spectra Physics, Newport, CA, USA) generating 800-nm pulses (pulse width between 35 and 50 fs, 4.0 mJ per pulse, at 1 kHz). The amplifier was pumped with of an Empower 30 Q-switched laser operated at 20 W (the second harmonic). A MaiTai SP oscillator provided the seed beam (55 nm bandwidth). The wavelength of the pump was tuned using an optical parametric amplifier, OPA-800CU (Newport Corporation, Newport, CA, USA), equipped with a second and fourth harmonic signal generators. For optimal OPA performance, the pulse duration from the amplifier was tuned to 50 fs. The signal was tuned to 1,560 nm and the power of the signal and the idler prior the second harmonic generator was stabilized at about 150 to 200 mW. The pulse after the fourth harmonic generator was fine-tuned to 390 nm, and the power was stabilized at 5 to 7 μJ per pulse.

The kinetics for the transient absorption and the emission decay data was extracted from least-square multiexponential data fits applied to decays at wavelengths corresponding to spectral peaks, as implemented using Igor Pro, v.6.36 (WaveMetrics, Inc., Lake Oswego, OR).

Acknowledgments

This work was supported by the US National Science Foundation (NSF), grant numbers CHE 1465284 (principal support), HRD 0932421 (for F. Z. and N. D.), CBET 0923408 (for the laser facilities), CHE 0541848 (for the UCR MS facilities), and DMR 1359136 (for M. W., summer support).

Keywords: Sensitizers · Triplet sensitizer · Fluorecent probes · Electron acceptor · Nitration · Conformational dynamics

[1] a) T. M. Figueira-Duarte, K. Müllen, *Chem. Rev.* **2011**, *111*, 7260–7314; b) V. I. Vullev, H. Jiang, G. Jones II, *Topics in Fluorescence Spectroscopy* **2005**, vol. 10, p. 211–239; c) F. Fages, S. Leroy, T. Soujanya, J.-E. Sohna Sohna, *Pure Appl. Chem.* **2001**, *73*, 411–414; d) M. E. Ostergaard, P. J. Hrdlicka, *Chem. Soc. Rev.* **2011**, *40*, 5771–5788; e) C. Wang, C. Wu, Y. Chen, Y. Song, W. Tan, C. J. Yang, *Curr. Org. Chem.* **2011**, *15*, 465–476; f) C. Bohne, M. Barra, R. Boch, E. B. Abuin, J. C. Scaiano, *J. Photochem. Photobiol. A* **1992**, *65*, 249–265.

[2] a) S. Perumal, B. Minaev, H. Aagren, *J. Chem. Phys.* **2012**, *136*, 104702/104701–104702/104716; b) E. San-Fabiin, F. Moscardo, *Int. J. Quantum Chem.* **2013**, *113*, 815–819.

[3] a) S. S. Babu, V. K. Praveen, A. Ajayaghosh, *Chem. Rev.* **2014**, *114*, 1973–2129; b) J. Duhamel, *Langmuir* **2012**, *28*, 6527–6538; c) S. Karuppannan, J.-C. Chambron, *Chem. Asian J.* **2011**, *6*, 964–984; d) E. Manandhar, K. J. Wallace, *Inorg. Chim. Acta* **2012**, *381*, 15–43; e) D. W. Johnson, K. N. Raymond, *Inorg. Chem.* **2001**, *40*, 5157–5161; f) M. I. Souza, Y. M. Jaques, G. P. de Andrade, A. O. Ribeiro, E. R. da Silva, E. E. Fileti, E. d. S. Avilla, M. V. B. Pinheiro, K. Krambrock, W. A. Alves, *J. Phys. Chem. B* **2013**, *117*, 2605–2614; g) W. Wang, S. Guo, M. Penchev, J. Zhong, J. Lin, D. Bao, V. Vullev, M. Ozkan, C. S. Ozkan, *J. Nanosci. Nanotechnol.* **2012**, *12*, 6913–6920.

[4] a) G. Jones II, V. Vullev, E. H. Braswell, D. Zhu, *J. Am. Chem. Soc.* **2000**, *122*, 388–389; b) G. Jones II, V. I. Vullev, *Org. Lett.* **2001**, *3*, 2457–2460; c) G. Jones II, V. I. Vullev, *J. Phys. Chem. A* **2001**, *105*, 6402–6406.

[5] a) G. Bains, A. B. Patel, V. Narayanaswami, *Molecules* **2011**, *16*, 7909–7935; b) J. Duhamel, *Polymers* **2012**, *4*, 211–239; c) N. Adamek, M. A. Geeves, *Experientia Suppl.* **2014**, *105*, 87–104.

[6] a) J. Martins, D. Arrais, M. Manuel, *Chem. Phys. Lipids* **2012**, *165*, 866–869; b) P. Somerharju, *Chem. Phys. Lipids* **2002**, *116*, 57–74; c) R. Saxena, S. Shrivastava, A. Chattopadhyay, *J. Phys. Chem. B* **2008**, *112*, 12134–12138; d) L. Le Guyader, C. Le Roux, S. Mazeres, H. Gaspard-Iloughmane, H. Gornitzka, C. Millot, C. Mingotaud, A. Lopez, *Biophys. J.* **2007**, *93*, 4462–4473; e) N. B. Karmen, N. P. Milyutina, A. A. Orlov, *Bull. Exp. Biol. Med.* **2005**, *139*, 562–564; f) M. Hashimoto, S. Hossain, S. Masumura, *Exp. Gerontol.* **1999**, *34*, 687–698; g) E. H. W. Pap, A. Hanicak, A. van Hoek, K. W. A. Wirtz, A. J. W. G. Visser, *Biochemistry* **1995**, *34*, 9118–9125.

[7] a) V. I. Vullev, G. Jones, *Tetrahedron Lett.* **2002**, *43*, 8611–8615; b) G. Jones II, X. Zhou, V. I. Vullev, *Photochem. Photobiol. Sci.* **2003**, *2*, 1080–1087; c) D. Bao, S. Upadhyayula, J. M. Larsen, B. Xia, B. Georgieva, V. Nunez, E. M. Espinoza, J. D. Hartman, M. Wurch, A. Chang, C.-K. Lin, J. Larkin, K. Vasquez, G. J. O. Beran, V. I. Vullev, *J. Am. Chem. Soc.* **2014**, *136*, 12966–12973.

[8] a) Y. Niko, S. Sasaki, S. Kawauchi, K. Tokumaru, G.-i. Konishi, *Chem. Asian J.* **2014**, *9*, 1797–1807; b) Y. Niko, Y. Cho, S. Kawauchi, G.-i. Konishi, *RSC Adv.* **2014**, *4*, 36480–36484; c) Y. Li, D. Wang, L. Wang, Z. Li, Q. Cui, H. Zhang, H. Yang, *J. Lumin.* **2012**, *132*, 1010–1014; d) Y. Niko, S. Kawauchi, G.-i. Konishi, *Chem. Eur. J.* **2013**, *19*, 9760–9765; e) R. Flamholc, D. Plazuk, J. Zakrzewski, R. Metivier, K. Nakatani, A. Makal, K. Wozniak, *RSC Adv.* **2014**, *4*, 31594–31601.

[9] a) C. Armbruster, M. Knapp, K. Rechthaler, R. Schamschule, A. B. J. Parusel, G. Kohler, W. Wehrmann, *J. Photochem. Photobiol. A* **1999**, *125*, 29–38; b) G. Jones II, V. I. Vullev, *Org. Lett.* **2002**, *4*, 4001–4004.

[10] a) Z. I. Garcia-Berrios, R. Arce, *J. Phys. Chem. A* **2012**, *116*, 3652–3664; b) R. Arce, E. F. Pino, C. Valle, J. Agreda, *J. Phys. Chem. A* **2008**, *112*, 10294–10304; c) C. E. Crespo-Hernandez, G. Burdzinski, R. Arce, *J. Phys. Chem. A* **2008**, *112*, 6313–6319; d) G. Jones II, L. N. Lu, V. Vullev, D. Gosztola, S. Greenfield, M. Wasielewski, *Bioorg. Med. Chem. Lett.* **1995**, *5*, 2385–2390.

[11] a) J. Singh, S. Singh, B. Shaik, O. Deeb, N. Sohani, V. K. Agrawal, P. V. Khadikar, *Chem. Biol. Drug Des.* **2008**, *71*, 230–243; b) T. Kameda, A. Akiyama, M. Yoshita, C. Tachikawa, A. Toriba, N. Tang, K. Hayakawa, *J. Health Sci.* **2011**, *57*, 372–377; c) Y.-W. Sun, F. P. Guengerich, A. K. Sharma, T. Boyiri, S. Amin, K. El-Bayoumy, *Chem. Res. Toxicol.* **2004**, *17*, 1077–1085; d) A. Toriba, H. Kitaoka, R. L. Dills, S. Mizukami, K. Tanabe, N. Takeuchi, M. Ueno, T. Kameda, N. Tang, K. Hayakawa, C. D. Simpson, *Chem. Res. Toxicol.* **2007**, *20*, 999–1007; e) K. N. Kirouac, A. K. Basu, H. Ling, *Nucleic Acids Res.* **2013**, *41*, 2060–2071; f) H. Jung, A. U. Shaikh, R. H. Heflich, P. P. Fu, *Environ. Mol. Mutagen.* **1991**, *17*, 169–180; g) A. Mayati, E. Le Ferrec, J. A. Holme, O. Fardel, D. Lagadic-Gossmann, J. Oevrevik, *Toxicol. In vitro* **2014**, *28*, 1153–1157.

[12] a) W. A. Lopes, P. A. d. P. Pereira, H. Viertler, J. B. de Andrade, *J. Braz. Chem. Soc.* **2005**, *16*, 1099–1103; b) B. Lu, J. Xu, C. Fan, F. Jiang, H. Miao, *Electrochim. Acta* **2008**, *54*, 334–340; c) R. Zahradnik, K. Bocek, *Collect. Czech. Chem. Commun.* **1961**, *26*, 1733–1748; d) J. Barek, J. Zima, J. C. Moreira, A. Muck, *Collect. Czech. Chem. Commun.* **2000**, *65*, 1888–1896.

[13] a) A. Musa, B. Sridharan, H. Lee, D. L. Mattern, *J. Org. Chem.* **1996**, *61*, 5481–5484; b) X. Zheng, M. E. Mulcahy, D. Horinek, F. Galeotti, T. F. Magnera, J. Michl, *J. Am. Chem. Soc.* **2004**, *126*, 4540–4542; c) T. Iwamoto, E. Kayahara, N. Yasuda, T. Suzuki, S. Yamago, *Angew. Chem. Int. Ed.* **2014**, *53*, 6430–6434; *Angew. Chem.* **2014**, *126*, 6548; d) T. Umemoto, S. Satani, Y. Sakata, S. Misumi, *Tetrahedron Lett.* **1975**, 3159–3162; e) R. G. Harvey, M. Konieczny, J. Pataki, *J. Org. Chem.* **1983**, *48*, 2930–2932; f) D. Rausch, C. Lambert, *Org. Lett.* **2006**, *8*, 5037–5040; g) H. Lee, R. G. Harvey, *J. Org. Chem.* **1986**, *51*, 2847–2848.

[14] a) T. Yamato, S. Ide, K. Tokuhisa, M. Tashiro, *J. Org. Chem.* **1992**, *57*, 271–275; b) D. M. Connor, S. D. Allen, D. M. Collard, C. L. Liotta, D. A. Schiraldi, *J. Org. Chem.* **1999**, *64*, 6888–6890; c) M. Tashiro, T. Yamato, K. Kobayashi, T. Arimura, *J. Org. Chem.* **1987**, *52*, 3196–3199.

[15] S.-S. Li, K.-J. Jiang, C.-C. Yu, J.-H. Huang, L.-M. Yang, Y.-L. Song, *New J. Chem.* **2014**, *38*, 4404–4408.

[16] a) A. G. Crawford, A. D. Dwyer, Z. Liu, A. Steffen, A. Beeby, L.-O. Palsson, D. J. Tozer, T. B. Marder, *J. Am. Chem. Soc.* **2011**, *133*, 13349–13362; b) S. Thekku Veedu, D. Raiser, R. Kia, M. Scholz, S. Techert, *J. Phys. Chem. B* **2014**, *118*, 3291–3297; c) K. Muellen, *Helv. Chim. Acta* **1978**, *61*, 2307–2317.

[17] a) P. Babu, N. M. Sangeetha, P. Vijaykumar, U. Maitra, K. Rissanen, A. R. Raju, *Chem. Eur. J.* **2003**, *9*, 1922–1932; b) M. Barfield, M. J. Collins, J. E. Gready, S. Sternhell, C. W. Tansey, *J. Am. Chem. Soc.* **1989**, *111*, 4285–4290.

[18] a) D. S. Ross, G. P. Hum, R. J. Schmitt, *Adv. Chem., Ser.* **1988**, *217*, 155–168; b) L. Eberson, F. Radner, *Acta Chem. Scand., Ser. B* **1985**, *B39*, 343–356; c) F. Radner, *Acta Chem. Scand., Ser. B* **1983**, *B37*, 65–67.

[19] E. Kupce, *Top. Curr. Chem.* **2013**, *335*, 71–96.

[20] a) O. Petersen Bent, E. Vinogradov, W. Kay, P. Wurtz, T. Nyberg Nils, O. Duus, J. W. Sorensen Ole, *Carbohydr. Res.* **2006**, *341*, 550–556; b) N. T. Nyberg, J. O. Duus, O. W. Sorensen, *J. Am. Chem. Soc.* **2005**, *127*, 6154–6155.

[21] a) D. Bao, B. Millare, W. Xia, B. G. Steyer, A. A. Gerasimenko, A. Ferreira, A. Contreras, V. I. Vullev, *J. Phys. Chem. A* **2009**, *113*, 1259–1267; b) D. Bao, S. Ramu, A. Contreras, S. Upadhyayula, J. M. Vasquez, G. Beran, V. I. Vullev, *J. Phys. Chem. B* **2010**, *114*, 14467–14479.

[22] a) A. K. Mora, S. Murudkar, P. K. Singh, N. S. K. Gowthaman, T. Mukherjee, S. Nath, *J. Photochem. Photobiol. A* **2013**, *271*, 24–30; b) S. Murudkar, A. K. Mora, P. K. Singh, S. Nath, *J. Phys. Chem. A* **2011**, *115*, 10762–10766; c) R. Arce, E. F. Pino, C. Valle, I. Negron-Encarnacion, M. Morel, *J. Phys. Chem. A* **2011**, *115*, 152–160.

[23] a) B. Xia, D. Bao, S. Upadhyayula, G. Jones, V. I. Vullev, *J. Org. Chem.* **2013**, *78*, 1994–2004; b) J. M. Larsen, E. M. Espinoza, V. I. Vullev, *J. Photon. Energy* **2015**, *5*, 055598; c) J. M. Larsen, E. M. Espinoza, J. D. Hartman, C.-K. Lin, M. Wurch, P. Maheshwari, R. K. Kaushal, M. J. Marsella, G. J. O. Beran, V. I. Vullev, *Pure Appl. Chem.* **2015**, published online ahead of print.

[24] a) F. Garo, R. Haener, *Angew. Chem. Int. Ed.* **2012**, *51*, 916–S916/911-S916/923, 919; *Angew. Chem.* **2012**, *124*, 940; b) K. Sen, S. Bandyopadhyay, D. Bhattacharya, S. Basu, *J. Phys. Chem. A* **2001**, *105*, 9077–9084; c) H. Inomata, H. Hamatani, N. Wada, Y. Yagi, S. Saito, *J. Phys. Chem.* **1993**, *97*, 6332–6333; d) A. Y. Sosorev, D. Y. Paraschuk, *Isr. J. Chem.* **2014**, *54*, 650–673; e) S. A. Zapunidy, D. S. Martyanov, E. M. Nechvolodova, M. V. Tsikalova, Y. N. Novikov, D. Y. Paraschuk, *Pure Appl. Chem.* **2008**, *80*, 2151–2161; f) A. A. Bakulin, S. A. Zapunidy, M. S. Pshenichnikov, P. H. M. van Loosdrecht, D. Y. Paraschuk, *Phys. Chem. Chem. Phys.* **2009**, *11*, 7324–7330; g) S. Laricchia, E. Fabiano, F. Della Sala, *J. Chem. Phys.* **2013**, *138*, 124112/124111–124112/124112; h) T.-W. Ng, M.-F. Lo, M.-K. Fung, W.-J. Zhang, C.-S. Lee, *Adv. Mater.* **2014**, *26*, 5569–5574.

[25] O. Taratula, J. Rochford, P. Piotrowiak, E. Galoppini, R. A. Carlisle, G. J. Meyer, *J. Phys. Chem. B* **2006**, *110*, 15734–15741.

[26] a) J. Guasch, L. Grisanti, M. Souto, V. Lloveras, J. Vidal-Gancedo, I. Ratera, A. Painelli, C. Rovira, J. Veciana, *J. Am. Chem. Soc.* **2013**, *135*, 6958–6967; b) X. Y. Shen, W. Z. Yuan, Y. Liu, Q. Zhao, P. Lu, Y. Ma, I. D. Williams, A. Qin, J. Z. Sun, B. Z. Tang, *J. Phys. Chem. C* **2012**, *116*, 10541–10547; c) Q. Zhang, H. Kuwabara, W. J. Potscavage, S. Huang, Y. Hatae, T. Shibata, C. Adachi, *J. Am. Chem. Soc.* **2014**, *136*, 18070–18081; d) G. Jones II, D. Yan, J. Hu, J. Wan, B. Xia, V. I. Vullev, *J. Phys. Chem. B* **2007**, *111*, 6921–6929; e) J. Wan, A. Ferreira, W. Xia, C. H. Chow, K. Takechi, P. V. Kamat, G. Jones, V. I. Vullev, *J. Photochem. Photobiol. A* **2008**, *197*, 364–374; f) J. Hu, B. Xia, D. Bao, A. Ferreira, J. Wan, G. Jones, V. I. Vullev, *J. Phys. Chem. A* **2009**, *113*, 3096–3107; g) J. P. Palmans, M. Van der Auweraer, A. Swinnen, F. C. De Schryver, *J. Am. Chem. Soc.* **1984**, *106*, 7721–7728.

[27] a) J. M. Vasquez, A. Vu, J. S. Schultz, V. I. Vullev, *Biotechnol. Prog.* **2009**, *25*, 906–914; b) S. Upadhyayula, V. Nunez, E. M. Espinoza, J. M. Larsen, D. Bao, D. Shi, J. T. Mac, B. Anvari, V. I. Vullev, *Chem. Sci.* **2015**, *6*, 2237–2251.

[28] a) S. Guo, D. Bao, S. Upadhyayula, W. Wang, A. B. Guvenc, J. R. Kyle, H. Hosseinibay, K. N. Bozhilov, V. I. Vullev, C. S. Ozkan, M. Ozkan, *Adv. Funct. Mater.* **2013**, *23*, 5199–5211; b) V. Nuñez, S. Upadhyayula, B. Millare, J. M. Larsen, A. Hadian, S. Shin, P. Vandrangi, S. Gupta, H. Xu, A. P. Lin, G. Y. Georgiev, V. I. Vullev, *Anal. Chem.* **2013**, *85*, 4567–4577.

[29] a) M. B. Smith, J. Michl, *Chem. Rev.* **2010**, *110*, 6891–6936; b) V. M. Nichols, M. T. Rodriguez, G. B. Piland, F. Tham, V. N. Nesterov, W. J. Youngblood, C. J. Bardeen, *J. Phys. Chem. C* **2013**, *117*, 16802–16810.

[30] a) V. I. Vullev, *J. Phys. Chem. Lett.* **2011**, *2*, 503–508; b) B. Bahmani, S. Gupta, S. Upadhyayula, V. I. Vullev, B. Anvari, *J. Biomed. Opt.* **2011**, *16*, 051303/051301–051303/051310; c) S. Upadhyayula, D. Bao, B. Millare, S. S. Sylvia, K. M. M. Habib, K. Ashraf, A. Ferreira, S. Bishop, R. Bonderer, S. Baqai, X. Jing, M. Penchev, M. Ozkan, C. S. Ozkan, R. K. Lake, V. I. Vullev, *J. Phys. Chem. B* **2011**, *115*, 9473–9490; d) S. Upadhyayula, T. Quinata, S. Bishop, S. Gupta, N. R. Johnson, B. Bahmani, K. Bozhilov, J. Stubbs, P. Jreij, P. Nallagatla, V. I. Vullev, *Langmuir* **2012**, *28*, 5059–5069; e) B. Bahmani, C. Y. Lytle, A. M. Walker, S. Gupta, V. I. Vullev, B. Anvari, *Int. J. Nanomed.* **2013**, *8*, 1609–1620.

[31] a) A. Vallee, V. Humblot, C.-M. Pradier, *Acc. Chem. Res.* **2010**, *43*, 1297–1306; b) H. Lu, D. Bao, M. Penchev, M. Ghazinejad, V. I. Vullev, C. S. Ozkan, M. Ozkan, *Adv. Sci. Lett.* **2010**, *3*, 101–109; c) U. K. Gautam, M. Ghosh, M. Rajamathi, R. Seshadri, *Pure Appl. Chem.* **2002**, *74*, 1643–1649; d) Y. Zhang, E. Galoppini, *ChemSusChem* **2010**, *3*, 410–428; e) M. Garcia-Iglesias, J.-J. Cid, J.-H. Yum, A. Forneli, P. Vazquez, M. K. Nazeeruddin, E. Palomares, M. Gratzel, T. Torres, *Energy Environ. Sci.* **2011**, *4*, 189–194.

Received: October 19, 2015
Published Online: November 17, 2015

